A spatially-resolved human brain proteome atlas for understanding function and disease

Qi Xiao[1,2*], Yuting Xie[1,2*], Meng Luo[3,7*], Hui Yang[4,5*], Zhengyi Yang[6*], Ming Chen[4*], Weirong Xiang[1,2], Jinlong Gao[1,2], Jing Yu[1,2], Wenhao Jiang[1,2], Weigang Ge[10], Jianfei Lu[3], Zongxiang Nie[1,2], Yaoting Sun[1,2], Xinrui Lin[1,2], Wei Liu[1,2], Xu Zheng[7], Ning Fan[7], Zhixiang Yang[1,2], Jingyu Gu[1,2], Fei Xu[8], Ed S. Lein[11], Tianzi Jiang[6,9#], Ying Mao [4,5#], Yan Li[3#], Tiannan Guo[1,2#]

[1]School of Medicine, School of Life Sciences, Westlake University, Hangzhou, Zhejiang, China.

[2]Westlake Center for Intelligent Proteomics, Westlake Laboratory of Life Sciences and Biomedicine, Hangzhou, Zhejiang, China.

[3]Songjiang Research Institute and Songjiang Hospital, Department of Anatomy and Physiology, College of Basic Medical Science, Shanghai Jiao Tong University School of Medicine, Shanghai 201600, China.

[4]Department of Neurosurgery, National Center for Neurological Disorders, Shanghai Key Laboratory of Brain Function Restoration and Neural Regeneration, Huashan Hospital, Fudan University, Shanghai 200040, China.

[5]State Key Laboratory of Medical Neurobiology and MOE MRIFrontiers Center for Brain Science, Institute for Translational Brain Research, Fudan University, Shanghai 200040, China.

[6] Beijing Key Laboratory of Brainnetome and Brain-Computer Interface, Institute of Automation, Chinese Academy of Sciences, Beijing 100190, China.

[7]Department of Anatomy, Dalian Medical University, Dalian 116044, China.

[8]College of Basic Medical Science South China University of Technology, Guangzhou 510641, China.

[9] Xiaoxiang Institute for Brain Health and Yongzhou Central Hospital, Yongzhou 425000, China.

[10] Westlake Omics Biotechnology Co., Ltd, Hangzhou, China.

[11]Allen Institute for Brain Science, Seattle, 98103, Washington, USA

* These authors contributed equally to this work.

For correspondence: Tiannan Guo, guotiannan@westlake.edu.cn; Yan Li, ly316@126.com; Ying Mao, maoying@fudan.edu.cn; Tianzi Jiang, jiangtz@nlpr.ia.ac.cn.

Abstract

While the brain performs specialized functions across distinct regions, the spatial organization of the human brain proteome remains largely uncharted. Here we present a comprehensive spatially-resolved proteome atlas of the human brain, analyzing over two thousand MRI-guided locations across four individuals. Proteome analysis integrated with transcriptomics reveals extensive post-transcriptional regulation, with cortical regions showing markedly higher protein diversity than transcript. Unsupervised molecular clustering defines distinct brain territories that transcend anatomical boundaries, instead reflecting metabolic demands and functional specialization patterns. Application to epilepsy brain tissue uncovered disrupted astrocyte metabolism, protein homeostasis and therapeutic targets including the seizure-associated purinergic receptor P2RX7. This resource bridges molecular and systems neuroscience to accelerate neurological drug discovery.

Introduction

The human brain's complexity arises from intricate molecular networks operating across functionally specialized regions[1,2]. Cortical regions are particularly critical for higher-order functions including language, executive control, and abstract reasoning. While transcriptomic atlases have mapped gene expression patterns extensively[3,4], these studies reveal minimal transcriptional variation across cortical areas. While single-cell transcriptomics demonstrated remarkable cell-type diversity within the cortex[5,6]. The presence of diverse cell types alongside uniform regional transcriptomes suggests that additional molecular layers contribute to cortical specialization. We pursued systematic proteomics as a complementary approach to transcriptomics for understanding cortical molecular architecture.

Drug discovery for central nervous system disorders remains particularly challenging, with success rates markedly lower than for other disease[7]. Epilepsy exemplifies this difficulty: although most seizures arise from cortical regions—especially the temporal lobes—therapeutic strategies that directly target cortical dysfunction remain scarce[8,9]. As proteins are the principal targets of most drugs, and their abundance often diverges from transcript levels due to widespread post-transcriptional regulation[10], comprehensive cortical proteomic profiling may uncover therapeutic targets overlooked by transcriptomics.

Decoding protein-level variations across cortical regions is crucial for precision therapies targeting cortical disorders. Application of mass spectrometry to human brain tissue now achieves both high-throughput processing and comprehensive proteome depth[11]. Recent proteomics studies have expanded our knowledge of brain molecular composition[4,12-15], with the latest achieving ~10,000 protein coverage across 13 brain regions[12]. However, with limited cortical sampling in existing studies, the spatial heterogeneity of the cortical proteome remains poorly defined, and systematic proteomic mapping across diverse cortical regions with precise spatial registration remains a critical gap. Additionally, sex differences and hemispheric asymmetries in brain structure and function[16,17] likely have molecular underpinnings that could explain differential disease susceptibility[18,19], yet proteomic comparisons across sexes and hemispheres are lacking.

Here, we present a spatially-resolved human brain proteome atlas documenting 2367 samples from 1384 magnetic resonance imaging MRI-guided sample sites across four neurologically healthy individuals using pressure cycling technology (PCT) and data-independent acquisition mass spectrometry (DIA-MS)[20] (**Figure 1a**). We integrated proteomic data with published transcriptomics and Brainnetome[2] connectivity patterns, and identified sex-specific and hemisphere-specific proteomic signatures. Our multi-omic integration yielded 51 brain clusters with distinct functional annotations. With the help of this resource, we applied this atlas to 90 epilepsy patient samples and uncovered 51 novel drug target candidates. Our work bridges molecular and systems neuroscience, providing a foundational resource for studying human brain function in particularly cortical regions and accelerating drug discovery in neurology.

Results

Brain sample collection, MRI-guided spatial mapping and proteomic profiling

We collected brain tissue specimens from two Chinese males and two Chinese females, with no history of neuropsychiatric or neuropathological conditions (**Figure S1a** and **Supplementary methods**). Each human brain was perfusion-fixed in formalin within ten hours postmortem. For proteomic analysis, 307–379 discrete cortical and subcortical sampling points were collected using a punch biopsy tool from both hemispheres of each brain, yielding a total of 1384 spatially resolved sample locations across the four individuals (**Supplementary Table 1**). Additionally, MRI was performed on each brain (see **Supplementary methods**) to obtain standardized spatial coordinates for sample localization (**Supplementary Table 1**). These native coordinates were then transformed to the Montreal Neurological Institute (MNI) coordinate space[21], enabling cross-brain comparisons and integration with public databases. Samples from the cortex was assigned to 186 subregions defined by the Brainnetome Atlas, which provides detailed parcellation based on both structural connectivity and functional activation patterns. This MRI-guided approach represents a critical advance over previous brain proteomics studies [4,12,14], enabling direct correlation between molecular signatures and functionally defined brain territories (**Figure S1b**).

To enhance spatial coverage of deep brain structures, we expanded sampling to include additional subcortical nuclei and the cerebellum. These regions were anatomically annotated according to the Paxinos and Watson human brain atlas[22]. The cortical regions were further separated into grey and white matter compartments, and selected regions was sampled in biological replicates, resulting in 2277 spatially resolved samples in total. In addition, we collected 90 brain tissue specimens from 49 individuals with epilepsy, spanning six regions implicated in seizure disorders: the frontal, temporal, parietal, and occipital lobes, as well as the amygdala and hippocampus (**Supplementary Table 1**).

We employed PCT coupled with DIA-MS for proteomic analysis of human brain tissue[23-25]. First, we built a spectral library that is the most comprehensive to date for human brain, containing 196,892 peptides from 12,768 proteins, which includes 3708 protein isoforms (**Figure S2 a-h**). Subsequently, all MRI-guided samples were analyzed using a high-resolution MS, which quantified 171,225 unique peptides corresponding to 11,772 protein

groups and 3295 protein isoforms. This comprehensive detection of protein isoforms across brain regions revealed extensive alternative splicing diversity. Plectin (PLEC) exemplified striking region-specific isoform expression, with PLEC 1e enriched in the cerebral cortex (1.2-fold) and PLEC 1 enriched in subcortical nuclei (1.9-fold), reflecting different cytoskeletal requirements between these anatomically distinct brain regions[26] (**Figure S4a and b)**.

To monitor and ensure data quality, we implemented multiple quality control checkpoints throughout the brain proteomics pipeline (**Figure S1c** and **Supplementary Methods**). Median coefficient of variation was 1% for technical replicates and 2.6% for biological replicates from matched brain regions (**Figure S2i**). The dynamic range spanned seven orders of magnitude, from histone protein to mRNA splicing molecules. Principal component analysis revealed that biological variables (brain region, sex, individual) explained 32.2% of total variance, while technical factors contributed 1.1% (**Figure S1 e and f**).

To investigate the cross-species difference we employ filter-aided expansion proteomics (FAXP)[27]. FAXP expands tissue before mass spectrometry-based proteomics to enhance spatial resolution. We profiled 98 samples from 9 mice, covering 14 anatomically defined regions based on the Allen Mouse Brain Atlas (**Figure 3c** and **Figure S5a**). Sampled regions included cortical areas (auditory cortex Au1, cingulate cortex, visual cortex V1), hippocampal subfields (CA1, CA2, CA3, dentate gyrus), thalamic nuclei (posterior complex Po, ventral posteromedial VPM, anterior nuclei ATN, medial geniculate MGN, lateral posterior LP, dorsal lateral geniculate DLG), and hypothalamus (**Supplementary Table 3**). All proteome data are available on our website at db.prottalks.com.

Motor cortex shows greatest hemispheric protein asymmetry

Analysis of hemispheric protein expression patterns provides molecular insights into functional brain lateralization. Our comparison of 121 paired left and right hemisphere samples revealed that the precentral gyrus (PrG), also known as the primary motor cortex, exhibited the highest degree of hemispheric protein asymmetry (**Figure 1b**), with 1725 proteins in caudal ventrolateral area showing significant differential expression (adjusted $p < 0.05$). The left hemisphere demonstrated significant upregulation of proteins associated with enhanced neuronal excitability and metabolic activity, including voltage-gated potassium channel subunits (KCNA2, KCNA5, KCNAB2), mitochondrial respiratory chain components (NDUFA2, ATP5F1A), and key metabolic enzymes (PDHB, GLUL) (**Figure 1d**). This protein profile suggests heightened synaptic transmission capacity and energy metabolism, consistent with the left motor cortex's role in fine motor control and sequential movement execution. In contrast, the right hemisphere showed preferential expression of transcriptional regulators (CBFA2T3, ZBTB11, ZNF865) and protein quality control machinery (APEH, DERL1, ABHD14A), indicate active gene expression regulation and cellular homeostasis processes. These hemispheric differences in protein expression provide molecular evidence for the functional specialization of motor cortical regions and suggest that lateralized motor behaviours may be supported by distinct underlying proteome landscapes that optimize each hemisphere for its specialized computational demands.

Sex-specific protein profiles reveal distinct metabolic strategies in cerebellum

Sex-based proteomic analysis revealed that both left and right cerebellar hemispheres showed significant sex-specific protein expression patterns that revealed distinct metabolic and cellular strategies (**Figure 1c**). Females demonstrated enhanced mitochondrial efficiency through upregulated fatty acid metabolism enzymes (CPT1A, FAH, HADHA, ACADS). Males exhibited rapid energy production via enhanced glycolytic activity and mitochondrial biogenesis (NMNAT1, ATP1A4, MRPS12/16/23), but with heightened neuroinflammatory signalling including complement system activation (C4B, CFH, C1QA) and pro-inflammatory mediators (IFI44L, TNFRSF21, DAXX) (**Figure S2l**). These distinct metabolic profiles suggest sex-specific vulnerabilities to metabolic stress and neuroinflammation in the cerebellum.

Human cortical regions exhibit enhanced protein-level molecular diversity

To characterize the molecular diversity across brain regions, we calculated relative protein expression levels for each sampled region. We integrated left and right hemisphere proteomic data to enable direct comparison with transcriptomic data, resulting in analyses across 121 consolidated brain regions. We employed the scoring algorithm for tissue-specific proteins developed by the Snyder group[28,29], enabling direct comparison across multi-omics datasets. Using this method, we identified 428 proteins showing significant regional enrichment (RE) per region (**Figure S3**). To investigate the concordance and discordance between protein and RNA expression in brain regions, we applied the region specificity score to the published transcriptome data[3]. Samples that aligned with the Brainnetome Atlas were selected for analysis. On average, 384 transcripts showed enrichment per region. Comparing RE proteins and RE transcripts in each brain region, we observed that the cerebral cortex exhibited a notably higher number of RE proteins, indicating greater heterogeneity at the protein level (**Figure 2a**). The cumulative number of RE proteins in cortical regions was approximately 1.6 times higher than that of transcripts (**Figure 2b**). Previous studies have reported a high consistency in cortical transcription levels[3], however, our data suggest that protein-level differences in the cortex reflect region-specific post-transcriptional regulation, reflecting the distinct functional demands of specialized cortical areas.

To validate our findings across species and demonstrate the conservation of protein-transcript relationships, we applied FAXP to generate spatially resolved mouse brain proteomics data. FAXP expands tissue samples ~4-fold before microdissection, enabling precise isolation of brain regions for mass spectrometry, and we collected 90 punched samples across 14 distinct mouse brain regions for proteomic analysis. For comparison with RNA sequencing data[30], we consolidated samples into five major regions: cortex, anterior hippocampus, posterior hippocampus, thalamus, and hypothalamus. Analysis of regional enrichment revealed notable interspecies differences. Human cortical regions showed predominantly protein-level variation with minimal transcript differences, whereas mouse cortical areas displayed equivalent numbers of region-enriched proteins and transcripts (**Figure 3a**). Strikingly, mouse hippocampus exhibited 3.7-fold more region-enriched proteins than transcripts, suggesting enhanced post-transcriptional specialization. This hippocampal protein diversity likely reflects rodent-specific adaptations for spatial navigation and memory processing.

Proteomics uncovers regulatory proteins with therapeutic opportunities

To examine region-specific patterns, we analyzed the habenula, a key node in depression-related circuits[31]. Our analysis revealed that membrane receptors exhibited higher concordance between protein and RNA levels, whereas transcription factors and epigenetic regulators showed greater discordance and demonstrated strong variation mainly at the protein level (**Figure 2c**). Functional annotation revealed that habenula-enriched proteins were particularly enriched for methyltransferases and acetylation-related proteins (**Figure 2d**).

The extensive post-transcriptional regulation of transcription factors and epigenetic regulators offers unique therapeutic opportunities. These proteins, crucial for memory formation and implicated in autism[32], Alzheimer's disease and schizophrenia[33], are controlled through protein stability, localization and modifications—mechanisms invisible to transcriptomics. Our proteomic data thus provides essential insights for developing drugs targeting these regulatory proteins.

Cross-species comparison of protein-transcript correlations revealed conserved patterns. As in humans, transcription factors and epigenetic regulators showed greater discordance and demonstrated strong variation mainly at the protein level in mouse brain. To determine whether transcription factors and epigenetic regulators show consistent correlation patterns across brain regions, we performed Pearson correlation analysis between relative protein and transcript expression values in mouse brain. The overall protein-mRNA correlation was median $r = 0.49$, with 14% of genes showing significant positive correlation and 9% showing significant negative correlation ($p < 0.05$) (**Figure S5c-d**). Among the genes showing significant positive correlation, neuronal signaling pathways were most prominently enriched (**Figure S5e and f**). These results demonstrate that the relationship between protein and transcript abundance is evolutionarily conserved across mammalian species, with neurotransmitter receptors (AMPA, GABA, and NMDA receptors) maintaining tight transcriptional control across species, while regulatory proteins such epigenetic regulators undergo extensive post-transcriptional regulation.

Cortical and subcortical regions exhibit divergent molecular similarity principles

Having established that cortical regions show enhanced protein diversity compared to transcripts, we next investigated whether this protein-level specialization translates into distinct organizational patterns across brain areas. To understand how molecular similarity relates to anatomical and functional organization, we analyzed the distribution of RE proteins and RE transcripts across all brain regions.

Analysis of region pairs sharing the most RE molecules (top 5%) revealed distinct organizational principles: regions sharing high proteomic similarity (>155 commonly RE proteins) were predominantly cortical pairs, reflecting the functional specialization of cortical areas through shared proteins (**Figure 4c**). This protein-based clustering likely reflects the shared computational demands of cortical processing, where similar protein machinery supports complex cognitive functions. In contrast, transcriptomic similarity (>137 shared RE transcripts) was highest between subcortical nuclei and in subcortical-cortical connections, suggesting that these evolutionarily conserved structures maintain similar foundational gene expression programs. This divergent pattern reinforces that cortical regions achieve

specialization primarily through protein-level regulation, while subcortical regions rely more heavily on shared transcriptional mechanisms.

Connective hub regions exhibit enhanced protein-level neurotransmitter processing

Brain regions vary in their connectivity patterns, with some regions serving as highly connected "hubs" that integrate information across multiple brain networks. To examine how protein expression relates to brain connectivity structure, we analyzed protein specialization across regions with different connectivity profiles.

We first examined connectivity-based molecular specialization. We quantified connectivity degrees for each of the 184 cortical regions by summing their strongly connected neighbors, using functional connectivity matrices derived from HCP resting-state fMRI data with matched cortical parcellation[2] (**Figure 4a and Figure S6a**). Hub regions, characterized by high connectivity degrees, would require enhanced molecular machinery to support their extensive neural communication demands.

Analysis of highly connected hub regions revealed specialized protein expression patterns that support enhanced information processing. Hub regions showed elevated expression of neurotransmitter-degrading enzymes (ALDH2, MAOA, MAOB) and synaptic adhesion molecules (NLGN1, NLGN3, GRIN1) at the protein level ($p < 0.01$), highlighting their role in regulating neurotransmitter dynamics and synaptic stability (**Figure 4b and Figure S6b**). At the transcript level, connectivity correlated with neurotransmitter receptors (GRIK2, GRID2, GRIA1) and signaling molecules (MAOA, MAOB, GNG10). These findings demonstrate that hub regions are equipped with both enhanced neurotransmitter clearance capacity and receptor sensitivity, emphasizing the critical role of proteomic adaptations in sustaining high levels of information flow.

Multi-omics clustering reveals 21 molecularly distinct brain territories

To systematically identify molecular territories that transcend classical anatomical boundaries, we performed unsupervised multi-omics clustering on spatially matched proteomic and transcriptomic datasets covering brain regions (**Figure 5a**). Following independent normalization and batch effect correction for each omics layer, we employed the MOVICS framework[34], which aggregates consensus clustering across multiple algorithms. The optimal cluster number of k=21 was determined based on silhouette width and Clustering Prediction Index (**Figure S7**).

The 21 Molecular Brain Territories (MBTs) revealed both alignment with classical networks and novel organizational principles. For example, MBT 19 completely overlapped with the visual network, while MBTs 5 and 9 corresponded to limbic system components (**Figure 5c**). MBT 11 encompassed regions of the central executive network, including entorhinal cortex, cingulate areas, and Brodmann areas 20 and 38—regions earliest affected in Alzheimer's disease. MBT 21 consisted exclusively of thalamic nuclei (**Supplementary table 4**). Behavioral domain analysis using BrainMap metadata revealed distinct functional specializations[35]: MBT 5 showed strong enrichment for emotion and cognition, MBT 19 for vision, and MBT 9 for cognition (**Figure S8b**). Cell-type enrichment analysis[36] demonstrated

that MBTs 5 and 11 were dominated by glutamatergic neurons, while MBT 19 showed mixed GABAergic and glutamatergic populations (**Figure S8a**).

Distinct molecular patterns define functional specialization across brain territories

Pathway analysis revealed how distinct molecular patterns align with regional functional specialization (**Figure 5b and S9**). Limbic and executive territories (MBTs 5, 9, 11) supporting emotion, cognition, and executive control maintained high expression of neurotransmitter diversity and synaptic plasticity machinery. These regions showed coordinated upregulation of serotonin signaling proteins (AKT3, BDNF, BRAF)—critical for mood regulation in limbic circuits—alongside glutamatergic components (GRIA4, GRIN2A, GRIN2B) essential for cognitive flexibility (**Figure 5d**). MBT 5, encompassing emotional processing regions, uniquely expressed high levels of GABAergic proteins (GABRA1, GABRA3, GABRB2, GABRB3), reflecting the inhibitory control required for emotional regulation. The sustained expression of reelin signaling and synaptic plasticity pathways in these territories supports their need for continuous adaptation to complex cognitive and emotional demands. This molecular complexity was matched with high metabolic investment. MBTs 5, 9 and 11 showed enhanced glucose metabolism proteins (ALDOA, ENO1, GNPDA1) and mitochondrial fission machinery (DNM2, GDAP1, MCU), reflecting the energetic cost of maintaining diverse neurotransmitter systems and plasticity mechanisms. MBT 11, which encompasses regions vulnerable to Alzheimer's disease, also showed elevated expression of pathways associated with Parkinson's and Huntington's diseases. This suggests that the high neurotransmission demands and associated metabolic stress required to maintain cognitive flexibility may contribute to the heightened susceptibility of these regions to neurodegeneration. Supporting this, MBTs 9 and 11 exhibited upregulation of microglial and astrocytic autophagy markers at the transcript level, reflecting cellular stress responses that, when dysregulated, may contribute to neurodegeneration.

In striking contrast, MBT 19 (visual network) exhibited a molecularly streamlined architecture befitting its specialized sensory function. This territory showed systematic downregulation of neurotransmitter and metabolic pathways while selectively maintaining RNA processing machinery (nucleoporins and snRNPs). This molecular profile suggests that primary sensory regions achieve functional efficiency through molecular specialization rather than flexibility, potentially explaining their relative resilience to age-related decline.

Subcortical territories displayed distinct metabolic adaptations reflecting their functional roles. MBTs 20 and 21, encompassing thalamus, epithalamus, and hypothalamus, showed preferential expression of fatty acid oxidation and peroxisomal lipid metabolism pathways, consistent with the metabolic homeostasis and circadian regulation functions of these regions. Within this metabolic framework, MBT 21 (thalamus) was further distinguished by enhance dopamine receptor expression, reflecting specialized functions in reward processing and motor control (**Figure S9**).

These molecular territories reveal a fundamental principle: brain regions balance metabolic investment with functional demands, with flexible cognitive regions maintaining costly but adaptive molecular machinery while specialized sensory regions achieve efficiency through streamlined molecular architectures.

Brain proteome atlas reveals extensive molecular perturbations in epilepsy

To demonstrate the translational value of our brain proteome atlas, we analyzed 90 brain tissue samples from 49 epilepsy patients across six regions: frontal, parietal, temporal, and occipital lobes, plus amygdala and hippocampus (**Figure 6a**). Obtaining healthy brain tissue for comparison remains challenging due to limited post-mortem availability and ethical constraints, making our reference atlas particularly valuable. Comparative analysis identified 2381 differentially expressed proteins (|Fold change| > 3, adjusted $p < 0.05$, **Figure S10a and b**), with 969 proteins consistently dysregulated across all regions. These conserved changes enriched for acute phase response, Rho family GTPases and axonal guidance pathways (**Figure S10c and d**), revealing core molecular perturbations in epilepsy.

To assess therapeutic potential, we cross-referenced dysregulated proteins with ChEMBL[37] and DrugBank[38] databases, identifying 736 potential drug targets (**Figure 6b**). Notably, 51 of these proteins are already targeted by FDA-approved anti-epileptic drugs, validating our approach. The remaining 685 unexplored targets represent substantial opportunities for expanding the therapeutic arsenal against epilepsy.

Brain proteome atlas facilitates prioritization of epilepsy drug targets

To identify mechanism-based targets for temporal lobe epilepsy (TLE), we performed weighted correlation network analysis (WGCNA) on TLE patient samples, revealing seven co-expression modules (**Figure S11a**). Comparison with healthy temporal lobe networks revealed poor preservation of two modules: Module 4 (integrin cell surface interactions) and Module 5 (fatty acid β-oxidation), both enriched for astrocyte markers (**Figure S11b**). This disruption of integrin signaling and metabolic homeostasis in astrocytes—key regulators of seizure propagation and neuroinflammation—suggests novel therapeutic avenues. Additional region-specific analysis revealed that hippocampal WGCNA showed poor preservation of Module 1, which was enriched for protein ubiquitination pathways, indicating that epilepsy exhibits region-specific proteostasis dysfunction (**Figure S11c**).

Based on these network disruptions, we prioritized drug targets using stringent criteria for TLE (**Figure S11d**): (i) significant differential expression in TLE, (ii) brain specific expression proteins, (iii) membership in disrupted modules 4 or 5, and (iv) druggability in ChEMBL/DrugBank. This approach identified 54 candidate targets, including three validated by current anti-epileptic drugs and 51 novel targets (**Figure S11e, Supplementary Table 7**).

Among the 51 novel targets, P2RX7 (purinergic receptor P2X7) was notably upregulated. P2RX7 activation by extracellular ATP released during seizures triggers neuroinflammation through IL-1β release and microglial activation, perpetuating epileptogenesis. The receptor also mediates excitotoxicity and blood-brain barrier disruption, creating a self-reinforcing cycle that promotes seizure recurrence and progression[39,40]. P2RX7, in particular, represents a promising therapeutic opportunity, with several compounds already in development including AZD-9056, CE-224535, and JNJ-54175446[38], which could potentially be repurposed for epilepsy treatment. These findings demonstrate how integrating spatial proteomics with network analysis can accelerate discovery of mechanism-based therapies, moving beyond symptomatic treatment toward targeting disease-driving molecular networks.

Discussion

We present the first comprehensive spatially-resolved proteome atlas of the human brain, quantifying 11,772 proteins across 2367 MRI-guided samples. This resource provides unprecedented coverage of functionally diverse cortical territories, revealing that cortical specialization emerges primarily through post-transcriptional mechanisms. A 1.6-fold greater diversity at the protein level compared to the transcriptome across cortical regions explains how anatomically similar areas can perform distinct functions despite transcriptional uniformity (**Figure 2**). This finding resolves the paradox of cortical functional diversity and identifies molecular vulnerabilities relevant to neurological disorders predominantly affecting cortical networks.

To validate our findings, we employed FAXP in mouse brain, a technique essential for accessing small anatomical structures impossible to sample conventionally. FAXP enabled precise isolation of 14 brain regions, including small thalamic nuclei. Owing to the limited resolution of the transcriptomic data available for comparison, the 14 mouse brain regions were consolidated into 5 broader regions for analysis. Nevertheless, our high-resolution proteomic data remain preserved as a fine-grained mouse brain proteome atlas, enabling future in-depth investigations. Cross-species comparison revealed that post-transcriptional regulation of synaptic proteins is evolutionarily conserved, yet regional implementation differs markedly between species (**Figure 3**), highlighting the importance of human-specific molecular atlases for therapeutic development.

Our bilateral sampling strategy revealed comprehensive proteomic insights into hemispheric specialization. Left motor cortex upregulated synaptic excitability and metabolic proteins supporting rapid motor execution, while right hemisphere enriched transcriptional regulators enabling adaptive motor planning (**Figure 1**). More striking were sex-specific cerebellar signatures: females exhibited enhanced mitochondrial efficiency through fatty acid oxidation, whereas males showed rapid glycolytic metabolism coupled with neuroinflammatory activation (**Figure 1c and Figure S2**). These metabolic differences provide molecular mechanisms for sex-biased disease susceptibility and mandate sex-stratified approaches in therapeutic development.

Integration with connectome data demonstrated that network topology drives molecular specialization. Hub regions maintaining high connectivity expressed specialized molecular machinery—neurotransmitter-degrading enzymes for signal termination and diverse receptors for integration—revealing how molecular composition enables network function (**Figure 4**). This structure-function relationship suggests that disrupting hub region proteomes would have cascading network effects, potentially explaining why certain proteins become therapeutic targets.

Our identification of 21 MBTs uncovered fundamental principles governing disease susceptibility. Territories supporting cognition and emotion maintained metabolically expensive machinery—diverse neurotransmitter systems and plasticity pathways—creating vulnerability to neurodegeneration. MBT 11, encompassing regions affected early in Alzheimer's disease, exemplified this trade-off between functional flexibility and metabolic sustainability (**Figure 5**). Conversely, primary sensory territories achieved efficiency through

molecular streamlining, potentially explaining their relative resilience to age-related decline. These molecular profiles enable prediction of disease vulnerability and suggest territory-specific therapeutic strategies.

Application to epilepsy demonstrated immediate translational value. Our network analysis identified disrupted astrocyte metabolism and integrin signaling as core pathophysiological mechanisms, yielding 51 novel drug targets beyond current therapeutics, including KCNT1, a potassium channel whose mutations cause severe epileptic encephalopathies (**Figure 6**). This success validates molecular territory-based drug discovery and suggests similar approaches for other neurological disorders. The identification of region-specific molecular disruptions enables precision targeting while minimizing off-target effects.

Several limitations merit consideration. Our cohort size, while providing unprecedented spatial coverage, cannot capture population-level variation. However, our study design prioritized comprehensive regional comparisons, and the convergent findings across all subjects, including greater protein than transcript diversity in cortex and 21 molecular territories, demonstrate that fundamental principles of brain organization are consistently detectable even with limited sample sizes. Future expansions should incorporate larger, diverse cohorts and integration with single-cell resolution to dissect cell-type contributions to regional signatures.

This atlas transforms our understanding of brain organization from anatomical to molecular principles. For neuroscience, it reveals how protein-level regulation enables functional specialization invisible to genomics. For systems biology, it demonstrates how molecular networks organize to support connectivity and computation. For therapeutics, it provides systematic frameworks for target identification and validation. For precision medicine, it enables molecular classification of brain disorders and prediction of treatment responses based on affected territories.

The resource will be made freely available through our web portal, enabling researchers worldwide to explore protein expression patterns, compare disease-affected regions, and identify therapeutic opportunities. Integration with emerging technologies—spatial transcriptomics, single-cell proteomics, and functional imaging—will further enhance resolution and utility.

This spatially-resolved human brain proteome atlas bridges molecular and systems neuroscience, revealing how protein-level organization underlies brain function. By uncovering principles of molecular specialization and demonstrating clinical translation through epilepsy target discovery, this work establishes foundations for understanding brain organization and developing precision therapeutics. As neurological disorders increasingly burden global health, molecular brain maps become essential tools for transforming disease understanding into targeted interventions.

References

1 Glasser, M. F. *et al.* A multi-modal parcellation of human cerebral cortex. *Nature* **536**, 171-178, doi:10.1038/nature18933 (2016).

2 Fan, L. *et al.* The Human Brainnetome Atlas: A New Brain Atlas Based on Connectional Architecture. *Cereb Cortex* **26**, 3508-3526, doi:10.1093/cercor/bhw157 (2016).

3 Hawrylycz, M. J. *et al.* An anatomically comprehensive atlas of the adult human brain transcriptome. *Nature* **489**, 391-399, doi:10.1038/nature11405 (2012).

4 Sjostedt, E. *et al.* An atlas of the protein-coding genes in the human, pig, and mouse brain. *Science* **367**, doi:10.1126/science.aay5947 (2020).

5 Siletti, K. *et al.* Transcriptomic diversity of cell types across the adult human brain. *Science* **382**, eadd7046, doi:10.1126/science.add7046 (2023).

6 Jorstad, N. L. *et al.* Comparative transcriptomics reveals human-specific cortical features. *Science* **382**, eade9516, doi:10.1126/science.ade9516 (2023).

7 Kesselheim, A. S., Hwang, T. J. & Franklin, J. M. Two decades of new drug development for central nervous system disorders. *Nat Rev Drug Discov* **14**, 815-816, doi:10.1038/nrd4793 (2015).

8 Chen, Z., Brodie, M. J., Liew, D. & Kwan, P. Treatment Outcomes in Patients With Newly Diagnosed Epilepsy Treated With Established and New Antiepileptic Drugs: A 30-Year Longitudinal Cohort Study. *JAMA Neurol* **75**, 279-286, doi:10.1001/jamaneurol.2017.3949 (2018).

9 Devinsky, O. *et al.* Epilepsy. *Nat Rev Dis Primers* **4**, 18024, doi:10.1038/nrdp.2018.24 (2018).

10 Liu, Y., Beyer, A. & Aebersold, R. On the Dependency of Cellular Protein Levels on mRNA Abundance. *Cell* **165**, 535-550, doi:10.1016/j.cell.2016.03.014 (2016).

11 Guo, T., Steen, J. A. & Mann, M. Mass-spectrometry-based proteomics: from single cells to clinical applications. *Nature* **638**, 901-911, doi:10.1038/s41586-025-08584-0 (2025).

12 Tushaus, J. *et al.* A region-resolved proteomic map of the human brain enabled by high-throughput proteomics. *EMBO J*, e114665, doi:10.15252/embj.2023114665 (2023).

13 Li, S. *et al.* Multiregional profiling of the brain transmembrane proteome uncovers novel regulators of depression. *Sci Adv* **7**, doi:10.1126/sciadv.abf0634 (2021).

14 Guo, Z. *et al.* A Global Multiregional Proteomic Map of the Human Cerebral Cortex. *Genomics Proteomics Bioinformatics* **20**, 614-632, doi:10.1016/j.gpb.2021.08.008 (2022).

15 Wang, L. *et al.* A cross-species proteomic map reveals neoteny of human synapse development. *Nature* **622**, 112-119, doi:10.1038/s41586-023-06542-2 (2023).

16 Guadalupe, T. *et al.* Differences in cerebral cortical anatomy of left- and right-handers. *Front Psychol* **5**, 261, doi:10.3389/fpsyg.2014.00261 (2014).

17 Ingalhalikar, M. *et al.* Sex differences in the structural connectome of the human brain. *Proc Natl Acad Sci U S A* **111**, 823-828, doi:10.1073/pnas.1316909110 (2014).

18 Baron-Cohen, S. *et al.* Why are autism spectrum conditions more prevalent in males? *PLoS Biol* **9**, e1001081, doi:10.1371/journal.pbio.1001081 (2011).

19 Ferretti, M. T. *et al.* Sex differences in Alzheimer disease - the gateway to precision medicine. *Nat Rev Neurol* **14**, 457-469, doi:10.1038/s41582-018-0032-9 (2018).

20 Guo, T. *et al.* Rapid mass spectrometric conversion of tissue biopsy samples into permanent quantitative digital proteome maps. *Nat Med* **21**, 407-413, doi:10.1038/nm.3807 (2015).

21 Evans, A. C. *et al.* Anatomical mapping of functional activation in stereotactic coordinate space. *Neuroimage* **1**, 43-53, doi:10.1016/1053-8119(92)90006-9 (1992).

22 Johnson, G. A., Calabrese, E., Badea, A., Paxinos, G. & Watson, C. A multidimensional magnetic resonance histology atlas of the Wistar rat brain. *Neuroimage* **62**, 1848-1856, doi:10.1016/j.neuroimage.2012.05.041 (2012).

23 Cai, X. *et al.* High-throughput proteomic sample preparation using pressure cycling technology. *Nat Protoc* **17**, 2307-2325, doi:10.1038/s41596-022-00727-1 (2022).

24 Guo, T. *et al.* Rapid mass spectrometric conversion of tissue biopsy samples into permanent quantitative digital proteome maps. *Nat Med* **21**, 407-413, doi:10.1038/nm.3807 (2015).

25 Cai, X. *et al.* PulseDIA: Data-Independent Acquisition Mass Spectrometry Using Multi-Injection Pulsed Gas-Phase Fractionation. *J Proteome Res* **20**, 279-288, doi:10.1021/acs.jproteome.0c00381 (2021).

26 Fuchs, P. *et al.* Targeted inactivation of a developmentally regulated neural plectin isoform (plectin 1c) in mice leads to reduced motor nerve conduction velocity. *J Biol Chem* **284**, 26502-26509, doi:10.1074/jbc.M109.018150 (2009).

27 Dong, Z. *et al.* Spatial proteomics of single cells and organelles on tissue slides using filter-aided expansion proteomics. *Nat Commun* **15**, 9378, doi:10.1038/s41467-024-53683-7 (2024).

28 Jiang, L. *et al.* A Quantitative Proteome Map of the Human Body. *Cell* **183**, 269-283 e219, doi:10.1016/j.cell.2020.08.036 (2020).

29 Wang, M., Jiang, L. & Snyder, M. P. AdaTiSS: A Novel Data-Adaptive Robust Method for Identifying Tissue Specificity Scores. *Bioinformatics* **37**, 4469-4476, doi:10.1093/bioinformatics/btab460 (2021).

30 Hahn, O. *et al.* Atlas of the aging mouse brain reveals white matter as vulnerable foci. *Cell* **186**, 4117-4133.e4122, doi:10.1016/j.cell.2023.07.027 (2023).

31 Xin, Q. *et al.* Neuron-astrocyte coupling in lateral habenula mediates depressive-like behaviors. *Cell* **188**, 3291-3309.e3224, doi:10.1016/j.cell.2025.04.010 (2025).

32 Levenson, J. M. *et al.* Regulation of histone acetylation during memory formation in the hippocampus. *J Biol Chem* **279**, 40545-40559, doi:10.1074/jbc.M402229200 (2004).

33 Dard, R. F., Dahan, L. & Rampon, C. Targeting hippocampal adult neurogenesis using transcription factors to reduce Alzheimer's disease-associated memory impairments. *Hippocampus* **29**, 579-586, doi:10.1002/hipo.23052 (2019).

34 Lu, X., Meng, J., Zhou, Y., Jiang, L. & Yan, F. MOVICS: an R package for multi-omics integration and visualization in cancer subtyping. *Bioinformatics* **36**, 5539-5541, doi:10.1093/bioinformatics/btaa1018 (2021).

35 Vanasse, T. J. *et al.* BrainMap VBM: An environment for structural meta-analysis. *Hum Brain Mapp* **39**, 3308-3325, doi:10.1002/hbm.24078 (2018).

36 Berglund, L. *et al.* A genecentric Human Protein Atlas for expression profiles based on antibodies. *Mol Cell Proteomics* **7**, 2019-2027, doi:10.1074/mcp.R800013-MCP200 (2008).

37 Mendez, D. *et al.* ChEMBL: towards direct deposition of bioassay data. *Nucleic Acids Res* **47**, D930-d940, doi:10.1093/nar/gky1075 (2019).

38 Knox, C. *et al.* DrugBank 6.0: the DrugBank Knowledgebase for 2024. *Nucleic Acids Res* **52**, D1265-d1275, doi:10.1093/nar/gkad976 (2024).

39 Engel, T. The P2X7 Receptor as a Mechanistic Biomarker for Epilepsy. *Int J Mol Sci* **24**, doi:10.3390/ijms24065410 (2023).

40 Di Virgilio, F., Dal Ben, D., Sarti, A. C., Giuliani, A. L. & Falzoni, S. The P2X7 Receptor in Infection and Inflammation. *Immunity* **47**, 15-31, doi:10.1016/j.immuni.2017.06.020 (2017).

41 Gao, H. *et al.* Accelerated Lysis and Proteolytic Digestion of Biopsy-Level Fresh-Frozen and FFPE Tissue Samples Using Pressure Cycling Technology. *J Proteome Res* **19**, 1982-1990, doi:10.1021/acs.jproteome.9b00790 (2020).

42 Demichev, V. *et al.* dia-PASEF data analysis using FragPipe and DIA-NN for deep proteomics of low sample amounts. *Nat Commun* **13**, 3944, doi:10.1038/s41467-022-31492-0 (2022).

43 Yao, Z. *et al.* A high-resolution transcriptomic and spatial atlas of cell types in the whole mouse brain. *Nature* **624**, 317-332, doi:10.1038/s41586-023-06812-z (2023).

44 Zhu, T. *et al.* ProteomeExpert: a Docker image-based web server for exploring, modeling, visualizing and mining quantitative proteomic datasets. *Bioinformatics* **37**, 273-275, doi:10.1093/bioinformatics/btaa1088 (2021).

Figure legend

Figure 1. Generation and characterization of the human brain proteome atlas.

a, Flowchart illustrating the comprehensive pipeline for generating the draft human brain proteome atlas. **b,** Bar plot depicting the number of significantly dysregulated proteins between left and right hemispheres (Student's t-test, Benjamini-Hochberg adjusted $p < 0.05$). Colors represent different brain regions: frontal lobe (FL), temporal lobe (TL), parietal lobe (PL), limbic lobe (LL), occipital lobe (OL), insular lobe (IL), subcortical nuclei, and cerebellum.

c, Bar plot showing the number of significantly dysregulated proteins of male vs. female subjects (Student's t-test, Benjamini-Hochberg adjusted $p < 0.05$). Orange bars represent left hemisphere regions; dark blue bars represent right hemisphere regions.

d, Heatmap displaying protein expression patterns for significantly dysregulated proteins in the PrG. Color scale represents z-score normalized protein expression levels, with orange indicating higher expression and dark purple indicating lower expression relative to the mean.

Figure 2. Regional expression patterns and functional characterization of proteins and transcripts across brain subregions.

a, Comparative analysis of regionally enriched (RE) proteins and transcripts across 121 anatomically defined brain subregions. Each pie chart represents a single subregion, with chart size proportional to the total number of RE proteins (specificity score > 0.93, 95th percentile threshold, ANOVA, Benjamini-Hochberg adjusted $p < 0.05$) plus RE transcripts (specificity score > 0.94, 95th percentile threshold, ANOVA, Benjamini-Hochberg adjusted $p < 0.05$) detected in that region. Yellow segments indicate genes with concordant regional enrichment at both protein and transcript levels (shared gene symbols); pink segments represent RE proteins without corresponding RE transcripts; blue segments represent RE transcripts without corresponding RE proteins. **b,** Bar plot quantifying the distribution of RE proteins (pink) and RE transcripts (blue) between cerebral cortex and subcortical nuclei. Numbers above bars indicate total counts for each category. **c,** Chord diagram illustrating the distribution of drug targets among RE proteins and RE transcripts specifically within the habenula nucleus. Drug target information was sourced from the ChEMBL database (downloaded April 25, 2025). **d,** Gene Ontology (GO) pathway enrichment analysis for habenular RE proteins and transcripts. Yellow segments represent biological pathways enriched in genes showing concordant regional enrichment at both protein and transcript levels; pink bars indicate pathways specifically enriched in RE proteins; blue bars represent pathways specifically enriched in RE transcripts.

Figure 3. FAXP data generation and analysis pipeline for region-resolved spatial proteomics.

a, Comparative analysis of RE proteins and transcripts across five major mouse brain regions: cortex, anterior hippocampus, posterior hippocampus, thalamus and hypothalamus. Transcriptomic data were obtained from a publicly available aging mouse brain bulk transcriptome dataset and integrated with our FAXP region-resolved proteomic data.

b, Functional annotation and drug target classification of RE proteins in the mouse cortex. Cortex-enriched proteins were categorized into functional classes including membrane receptors, ion channels, transporters, enzymes, transcription factors, and other protein types.

c, Schematic overview of the FAXP experimental pipeline. The methodology encompasses: (1) mouse brain tissue collection from nine brains across two age groups (11-month: 2 males, 2 females; 24-month: 3 males, 2 females), (3) hydrogel embedding and tissue expansion, (4) Coomassie blue staining, (2) anatomical region mapping using the Allen Brain Atlas reference, and (5) region-specific sample collection yielding 14 samples covering both hemispheres.

Figure 4. Integration of proteomics data with brain structural connectome analysis.

a, Bar plot shows connectivity degrees for each cortical region, quantified by summing strongly connected neighbors using functional connectivity matrices derived from HCP resting-state fMRI data with matched cortical parcellation. Dark bars represent left hemisphere regions; light bars represent right hemisphere regions. Higher values indicate greater functional connectivity with neighboring regions. **b,** Pathway enrichment (IPA) analysis for genes showing positive correlations with connectivity degree. Red circles represent pathways enriched in positively correlated proteins; blue circles represent pathways enriched in positively correlated transcripts. **c,** Network visualization of the top 5% of subregion pairs sharing the highest number of RE proteins and transcripts. Circle size represents the total number of RE proteins and RE transcripts detected in each subregion. Curved lines connect subregion pairs within the top 5% for shared RE features.

Figure 5. Molecular-based brain parcellation reveals functional organization patterns.

a, Consensus clustering of 216 brain subregions into 21 MBTs. The consensus heatmap displays the consensus index for each subregion. **b,** Bar plot displaying the number of differentially expressed proteins (red) and transcripts (dark blue) for each of the 21 MBTs. Each cluster compared to all other clusters combined. Significance thresholds were set at Benjamini-Hochberg adjusted $p < 0.05$ and $|\text{fold-change}| > 1.5$. **c,** Three-dimensional visualization of MBTs mapped onto standard brain anatomy. Views shown include lateral, medial, and ventral perspectives of both hemispheres. **d,** Heatmap showing differential gene expression profiles across 21 MBTs. Each row represents an MBT and each column represents a gene. Values indicate log2 fold change of gene expression in each MBT compared to all other MBTs combined. Red indicates upregulation and blue indicates downregulation.

Figure 6. Anti-epilepsy drug target screening through region-specific dysregulation analysis.

a, Pipeline for epilepsy drug target discovery. Epileptic brain proteome data were integrated with corresponding brain region data from our healthy brain database, yielding a total of 1002 samples for analysis. Protein expression matrices from brain tissues of healthy individuals and epileptic patients were analyzed using WGCNA, specifically comparing healthy temporal lobe versus epileptic temporal lobe samples. **b,** Sankey diagram illustrating the regional distribution and drug target classification of 736 potential drug targets, including 51 proteins that are targets of FDA-approved anti-epileptic drugs. The flow shows: (left) dysregulated

potential drug targets, (middle) number of brain regions where each protein is dysregulated, and (right) drug target classification. Drug target annotations were obtained from ChEMBL and DrugBank databases (ChEMBL downloaded April 25, 2025; DrugBank downloaded April 29, 2025).

Methods

Formalin-fixed brain sample collection and MRI imaging

Human brain samples were collected from Dalian Medical University Body and Organ Donation Center. The human brains were formalin-fixed within 10 hours of death. The samples originated from two male and two female donors. Brain punches were taken from the cerebral cortex, subcortical nuclei, and cerebellum. Furthermore, the cerebral cortex samples were segmented into white and grey matter. After sampling, the MRI scanning of the brain was performed to obtain the spatial coordinates of all the sampling locations. The donations are handled in accordance with ethical guidelines and regulations. These samples were then transported to the laboratory for proteomic analysis.

Proteomic sample processing and data profiling

For proteome data profiling, we employed PCT-assisted sample preparation[23,24,41] and PulseDIA mass spectrometry data acquisition[25]. PCT utilizes alternating cycles of high pressure and ambient pressure to enhance protein extraction efficiency from small tissue volumes, particularly important for extracting membrane proteins and proteins from compact tissue structures. This method enabled complete protein solubilization from biopsy-level samples (1-2 mg) while maintaining protein integrity. The procedures involved deparaffinization and rehydration of the formalin-fixed brain tissue samples, followed by PCT treatment to enhance protein extraction and digestion efficiency. Then, the samples were desalted. The resulting peptide mixture was analyzed using a hybrid quadrupole-Orbitrap mass spectrometer coupled with a nanoflow-performance liquid chromatography system.

To investigate cross-species differences, we employed FAXP, which combines tissue expansion with protein staining to visualize cytoarchitectural boundaries, allowing accurate punch needle sampling of specific anatomical regions that would be challenging to isolate in unexpanded tissue.

Hybrid spectral library generation

For spectral library construction, we combined 354 data-dependent acquisition (DDA) runs from fractionated pooled brain tissue with 5362 DIA analyses from individual samples. The DDA runs utilized high-pH reverse-phase fractionation to increase proteome coverage (**Figure S1a**). To generate the hybrid spectral library, we employed MSFragger[42] and utilized both PulseDIA and DDA files. First, DIA-Umpire generated pseudo-MS/MS spectra from the DIA files. Subsequently, we used MSFragger in DDA mode for the library generation. The default settings were applied, including the generation of decoys and contaminants. Additionally, the ciRT peptide sequences contained in FragPipe were used for retention time normalization. For retention time correction during library generation, the option "ciRT" was utilized. The library was filtered to achieve a 1% false discovery rate at both the protein and

peptide levels. The FASTA file, consisting of a reviewed human Swiss-Prot sequence database containing canonical and isoform sequences (51,548 entries), was downloaded from UniProt (https://www.uniprot.org/).

Proteome and transcriptome integration.

We downloaded and processed Allen Brain Atlas microarray data from six neurotypical donors, comprising expression profiles for approximately 20,000 genes across multiple brain regions, to enable the comparison between protein and mRNA expression patterns across matched brain locations[43]. Allen Brain samples were matched to MNI coordinates using their documented stereotactic positions, enabling spatial alignment with our proteomic data. Brainnetome Atlas connectivity matrices were integrated to assign functional network membership to each sample. Data harmonization included gene identifier mapping, batch correction using ComBat[44].

Quality Control

Checkpoints Q1–Q3 were established to verify sample accuracy, while Q5–Q11 monitored sample preparation and data acquisition steps to maintain data quality (**Figure S1c**). Batch effects were minimized through stratified sampling process and inclusion of pooled quality control samples every 15 injections (**Figure S1d**).

More details are provided in Supplementary Methods.

Data availability

Our data are freely accessible via the website: https://db.prottalks.com

Our raw data have been deposited in the iProX database (https://www.iprox.cn/page/PSV023.html;?url=1754291881848RS9L

, project ID: IPX0008436000, password: HV28).

Password: HV28

Acknowledgments

We would like to express our gratitude to the National Key R&D Program of China (Grant No. 92259201, 2023C03056 and 2021ZD0200200). We are also grateful to the patients participated in this project for their donation of body or body tissue for scientific research. We also appreciate the advanced computing services provided by Westlake University High-Performance Computing Center.

Author contributions

Conceptualization: T. G., Y. L., T. J., and Y. M. Methodology: T. G., T. J. and Y. L. Investigation: Q. X., Y. X., M. L., Z. Y., J. Gao., J. Y., W. J., and W. G. Resources: Y. L., Y. M., L. C., H. Y., M. L., X. Z., N. F., and F. X. Data analysis: Q. X., Y. X., Z. Y., J. Y., W. J., W. G., J. L., W. L., and J. G. Visualization: Q. X., Y. X., Z. N., Y. C., and Z. F. Writing-

origin draft: Q. X., Y. X., and J. Gao. Writing-review & editing: T. G., T. J., E. S. L., Z. Y., and Y. S.

Competing interests

T. G. is a shareholder of Westlake Omics Inc. The remaining authors declare no competing interests.

Additional information

Supplementary Information is available for this paper. Correspondence and requests for materials should be addressed to Tiannan Guo, guotiannan@westlake.edu.cn.

Supplementary figure legend

Figure S1. Study design and quality control workflow, related to Figure 1.

a, Comprehensive data generation and analysis pipeline overview. Brain tissue collection encompassed four donors (two male, two female), with 307-379 tissue punches collected per brain (total n = 2367 samples). Cerebral cortex samples were anatomically separated into white and grey matter prior to paraffin embedding. Additionally, 90 epileptic brain grey matter samples were collected for comparative proteomic analysis. MRI scanning was performed to obtain precise spatial coordinates for all sampling locations of four donor brains, which were subsequently mapped to the Brainnetome Atlas reference framework. Paraffin-embedded specimens were processed to obtain 0.6-1.0 mg samples for PCT-assisted protein extraction and enzymatic digestion. The mass spectrometry workflow employed a DDA-DIA hybrid approach: DIA-Umpire generated pseudo-MS/MS spectra from DIA files, and DIA-NN executed library-based peptide identification and quantification. **b,** The 3D brain reconstruction shows sampling locations (indicated by green arrows) that correspond exactly to anatomical positions in the accompanying photograph. The three orthogonal MRI views (sagittal, horizontal, and coronal planes) demonstrate the spatial precision achieved for each sampling point, enabling accurate anatomical assignment and coordinate mapping. **c,** Dataset variance decomposition analysis using principal component analysis. The pie chart illustrates the relative contributions of different variance sources: biological variables (brain region, sex, individual differences). **d,** Uniform Manifold Approximation and Projection dimensionality reduction visualization of the complete proteomic dataset. Each point represents a single brain sample. **e,** Batch design strategy for systematic brain sample analysis to minimize technical variation. Each analytical batch contained: one pooled quality control sample, 15 brain tissue samples, one human cell line sample for process monitoring, and two technical replicates, ensuring balanced representation and robust quality assessment. **f,** Quality control checkpoint workflow integrated throughout the experimental pipeline. Green diamond symbols (Q) indicate mandatory quality control steps implemented between major processing stages. Comprehensive quality control procedures are detailed in Supplementary Methods 1, Section VI (Quality Control), covering sample collection, processing, mass spectrometry acquisition, and data analysis validation steps.

Figure S2. Characterization of the spectral library of human brain and quatification of proteome data, related to Figure 1.

a, Mass-to-charge ratio (m/z) distribution of peptide precursors in spectral library. **b,** Distribution of precursor ion charge states detected in the spectral library. **c,** Quality assessment of retention time alignment using indexed retention time (iRT) correction. **d,** Distribution of identified peptide lengths in the spectral library. **e,** Frequency analysis of post-translational modifications detected in the dataset. Bar chart displays counts for three major modifications: methionine oxidation (Δmass +16 Da), N-terminal acetylation (Δmass +42 Da), and cysteine carbamidomethylation (Δmass +57 Da. **f,** Distribution of proteotypic peptides per protein in the spectral library. **g,** Fragment ion coverage analysis showing the number of fragment ions per precursor. **h,** Charge state distribution of fragment ions observed in MS/MS spectra. **i,** Reproducibility assessment across different sample types. Left panel shows Pearson correlation coefficients; right panel displays coefficients of variation (CV) for

quality control pooled samples, technical replicates, and biological replicates. **j,** Principal component analysis of dataset variance across three mass spectrometry instruments. Scatter plots show PCA clustering before (left) and after (right) batch effect correction, with colors representing different instruments. **k,** Protein quantification coverage across all brain subregions. Bar chart displays the number of quantified proteins in each anatomical region. Colors represent different brain divisions: FL, TL, PL, LL, OL, IL, subcortical nuclei, and cerebellum. **l,** Heatmap displaying protein expression patterns for significantly dysregulated proteins in the cerebellum. Color scale represents z-score normalized protein expression levels, with orange indicating higher expression and dark purple indicating lower.

Figure S3. RE proteins and transcripts distribution across brain subregions, related to Figure 2.

Regional distribution of RE features across anatomically defined brain subregions. Left panel: number of RE proteins enriched in grey matter across 121 subregions, using specificity score > 0.93 (95th percentile threshold of the protein expression matrix) and ANOVA with Benjamini-Hochberg adjusted $p < 0.05$. Middle panel: number of RE transcripts enriched in grey matter across the same 121 subregions, based on microarray expression data from the Allen Human Brain Atlas, using specificity score > 0.94 (95th percentile threshold of the transcript expression matrix) and ANOVA with Benjamini-Hochberg adjusted $p < 0.05$. Right panel: number of RE proteins enriched in white matter across 94 subregions, applying identical protein enrichment criteria.

Figure S4. Correlations between transcript and protein abundance in the human brain, related to Figure 2.

a, Regional expression analysis of Plectin protein isoforms across brain subregions. Four Plectin isoforms (Plectin 1, Plectin 1e, Plectin 1a, and Plectin X7) were quantified across 121 anatomically defined subregions. **b,** Brain region heatmap displaying mean expression levels of the four Plectin isoforms across major anatomical divisions: FL, TL, PL, LL, OL, IL, subcortical nuclei, and cerebellum. Color intensity represents relative expression levels. **c,** Global correlation analysis between transcript and protein abundances across all brain samples. **d,** Protein category-specific correlation patterns between transcript and protein levels. Left panel displays the median Pearson correlation coefficient for each category. **e,** Pathway enrichment (IPA) analysis of genes showing significantly positive transcript-protein correlations. Bar plot displays the most statistically significant pathways (ranked by p-value), with color intensity representing the ratio of correlated genes within each pathway relative to total pathway size. **f,** Pathway enrichment (IPA) analysis of genes exhibiting significantly negative transcript-protein correlations. IPA analysis identified biological pathways enriched among negatively correlated genes. Bar plot shows the most statistically significant pathways (ranked by p-value), with color intensity indicating the ratio of negatively correlated genes within each pathway.

Figure S5. Correlations between transcript and protein abundance in the mouse brain, related to Figure 3.

a, FAXP sample collection, left of the panel: Nissl-stained mouse brain section after tissue expansion, with sampling sites indicated by circles representing 1 mm punch needle

collection points. Right of the panel: corresponding Allen Mouse Brain Atlas anatomical map showing regional segmentation and anatomical boundaries. **b,** Uniform Manifold Approximation and Projection dimensionality reduction visualization of the complete mouse FAXP proteomic dataset. Each point represents a single brain sample, demonstrating clustering patterns based on proteome profiles. **c,** Global correlation analysis between transcript and protein abundances across all brain samples. Of the analyzed genes, 14% exhibited significant positive correlations, while 1% showed significant negative correlations (Benjamini-Hochberg adjusted $p < 0.01$), with an overall mean Pearson correlation coefficient of 0.49. **d,** Protein category-specific correlation patterns between transcript and protein levels. Left panel displays the median Pearson correlation coefficient for each category. **e,** Pathway enrichment (IPA) analysis of genes showing significantly positive transcript-protein correlations. rBar plot displays the most statistically significant pathways (ranked by p-value), with color intensity representing the ratio of correlated genes within each pathway relative to total pathway size. **f,** Pathway enrichment (IPA) analysis of genes exhibiting significantly negative transcript-protein correlations. Bar plot shows the most statistically significant pathways (ranked by p-value), with color intensity indicating the ratio of negatively correlated genes within each pathway.

Figure S6 Structural connectivity patterns visualized through connectograms, related to Figure 4.

a, Connectogram displaying structural connectivity patterns for the left hemisphere area A8m (medial frontal area 8). Connecting lines represent strong structural connections between left A8m and other brain subregions, based on diffusion tensor imaging tractography data from the Brainnetome connectome atlas. Complete connectograms for all brain regions analyzed in this study are available through the Brainnetome Atlas website (https://atlas.brainnetome.org/). **b,** Scatter plots demonstrating the correlation between structural connectivity degree and protein expression levels across brain subregions. Connectivity degree calculated as the sum of strongly connected subregions for each given subregion. Each point represents a single subregion. Spearman correlation coefficients (rho) and Benjamini-Hochberg adjusted p-values are indicated at the top of each panel. **c,** Scatter plots showing the correlation between structural connectivity degree and transcript expression levels across brain subregions. **c,** Box plots comparing correlation strengths between highly connected brain subregion pairs across different gene functional categories. Proteins and transcripts were classified into eight functional groups: All, Ion channel, Secreted, Membrane receptor, Transporter, Enzyme, Transcription factor, Epigenetic regulator.

Figure S7 Molecular-based brain parcellation, related to Figure 5.

a, Consensus clustering optimization analysis showing the relationship between consensus scores and cluster number (K) across a range of K=1 to 45. **b,** Silhouette analysis validation of the 21-cluster solution. The silhouette plot demonstrates cluster quality with an average silhouette width of 0.46. Each bar represents an individual brain subregion, with positive values indicating good cluster assignment and negative values suggesting potential misclassification. **c,** Cluster composition and subregion assignment overview. Line plot connecting subregion names (left) to their assigned molecular clusters (right, numbered 1-21).

Figure S8 Neuronal signalling, development, and support pathway analysis, related to Figure 5.

a, Cell-type enrichment analysis for each of the 21 molecular clusters using established cell-type markers from the Human Protein Atlas (HPA). Enrichment scores were calculated using clusterProfiler. The heatmap shows enrichment scores for different cell types across clusters, with asterisks (*) marking statistically significant enrichments ($p < 0.05$, Fisher's exact test). **b,** Functional behavioral domain enrichment analysis across the 21 molecular clusters. Ridge plot shows the distribution of enrichment scores (calculated using clusterProfiler) for each cluster across 42 behavioral domain profiles from the BrainMap database (brainmap.org)[35]. Enrichment significance was determined using Fisher's exact test with $p < 0.05$.

Figure S9. Functional pathway analysis reveals territory-specific biological programs, related to Figure 5.

Ingenuity Pathway Analysis (IPA) activation z-scores for major biological themes across MBTs. Pathways are grouped into five functional categories: neurotransmitter signaling, brain development, energy metabolism, lipid metabolism, and immune response. Red indicates pathway activation (positive z-score) and blue indicates suppression (negative z-score).

Figure S10. Differential protein analysis between epileptic and healthy brains across six brain regions, related to Figure 6.

a, Volcano plots displaying dysregulated proteins in six brain regions (Temporal lobe, Hippocampus, Amygdala, Frontal lobe, Parietal lobe, Occipital lobe). Points outside the significance thresholds ($|\text{Fold change}| > 3$, Benjamini-Hochberg adjusted $p < 0.05$, Wilcoxon test) represent dysregulated proteins in epileptic versus healthy brain tissue. **b,** Bar plot quantifying proteomic coverage and dysregulation across the six brain regions. For each region, bars show the total number of proteins quantified (grey bars) and the subset of significantly dysregulated proteins in epileptic samples. **c,** UpSet diagram illustrating the overlap of dysregulated proteins across the six brain regions. **d,** Canonical pathway enrichment analysis of the 969 dysregulated proteins shared across all six brain regions using IPA.

Supplementary Figure S11. Anti-epilepsy drug target identification through co-expression network analysis, related to Figure 6.

a, WGCNA of epileptic temporal lobe samples revealing seven distinct protein co-expression modules. Each module represents a group of proteins with highly correlated expression patterns. Canonical pathway analysis using IPA identified the biological processes associated with each module. Cell-type specificity was assessed through enrichment analysis using neuron- and glia-specific protein markers from the HPA. **b,** Module preservation analysis comparing epileptic TL protein networks with healthy TL networks. Modules with preservation Z-summary scores < 2 were considered non-preserved (indicating epilepsy-specific disruption). Modules with Z-summary scores ≥ 2 (blue dotted line) were considered preserved, while those with scores ≥ 10 (red dotted line) were highly preserved. X-axis represents the number of proteins in each module. **c,** Module preservation analysis comparing

epileptic temporal lobe protein networks with epileptic hippocampus networks. This cross-regional comparison identifies modules that are specifically disrupted in temporal lobe epilepsy versus those representing general epilepsy-associated changes. Preservation thresholds are identical to panel b: Z-summary < 2 (non-preserved), ≥ 2 (preserved, blue line), and ≥ 10 (highly preserved, red line). **d,** Systematic drug target selection criteria for epileptic temporal lobe therapy. **e,** Expression validation of identified drug targets in temporal lobe samples. Box plots display the relative expression levels ($\log_2$ intensity from mass spectrometry) of 54 candidate drug targets comparing epileptic versus healthy temporal lobe samples. Wilcoxon test Benjamini-Hochberg adjusted p-values are labeled above each comparison. Targets with brown background represent the three proteins that are targets of currently approved anti-epileptic drugs.

Fig. 1

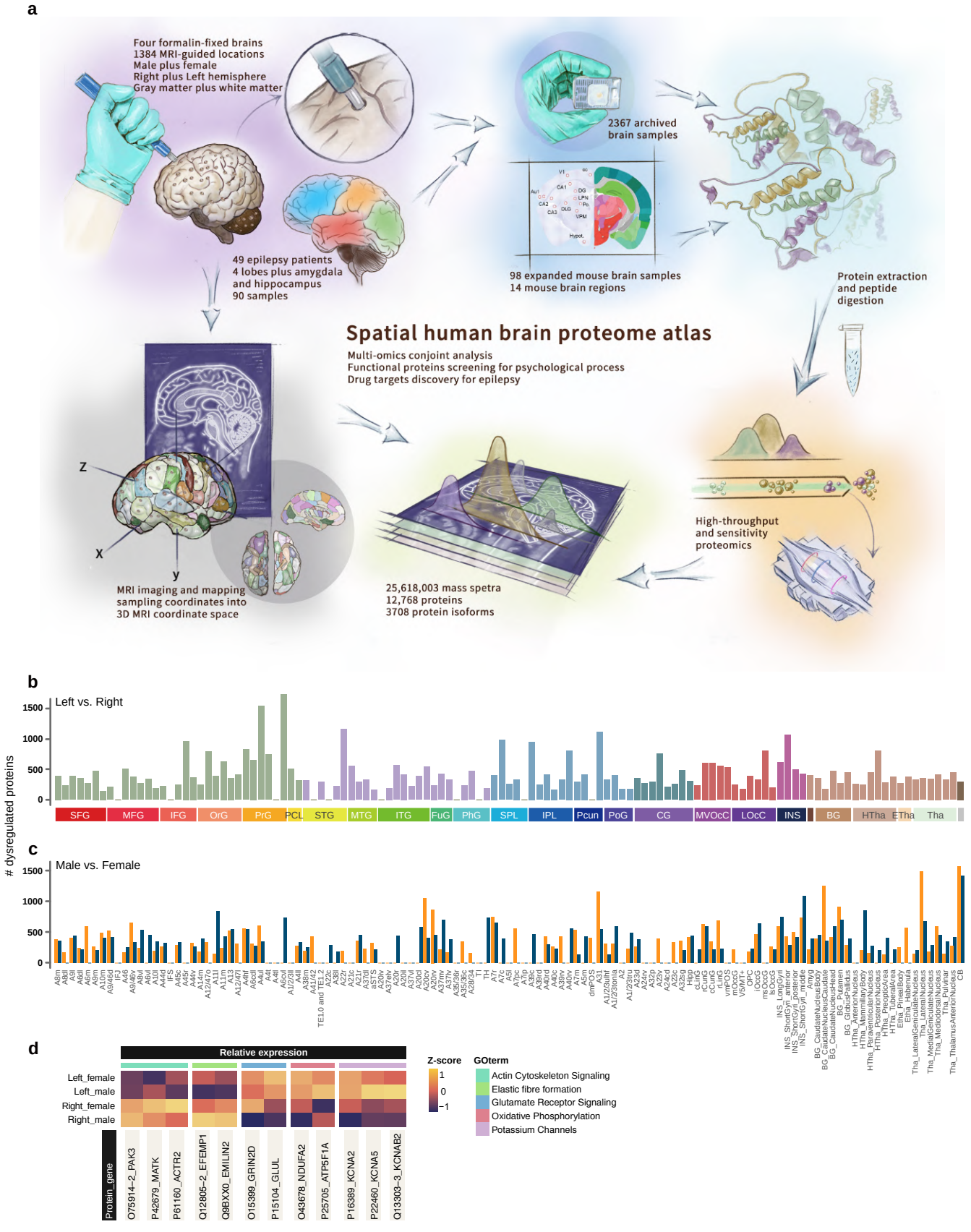
a
Four formalin-fixed brains
1384 MRI-guided locations
Male plus female
Right plus Left hemisphere
Gray matter plus white matter
2367 archived brain samples
49 epilepsy patients
4 lobes plus amygdala
and hippocampus
90 samples
98 expanded mouse brain samples
14 mouse brain regions
Protein extraction
and peptide
digestion
Spatial human brain proteome atlas
Multi-omics conjoint analysis
Functional proteins screening for psychological process
Drug targets discovery for epilepsy
Z
X
y
MRI imaging and mapping
sampling coordinates into
3D MRI coordinate space
25,618,003 mass spetra
12,768 proteins
3708 protein isoforms
High-throughput
and sensitivity
proteomics
b
Left vs. Right
dysregulated proteins
1500
1000
500
0
SFG
MFG
IFG
OrG
PrG
PCL
STG
MTG
ITG
FuG
PhG
SPL
IPL
Pcun
PoG
CG
MVOcC
LOcC
INS
BG
HTha
ETha
Tha
c
Male vs. Female
1500
1000
500
0
d
Relative expression
Left_female
Left_male
Right_female
Right_male
Protein_gene
O75914−2_PAK3
P42679_MATK
P61160_ACTR2
Q12805−2_EFEMP1
Q9BXX0_EMILIN2
O15399_GRIN2D
P15104_GLUL
O43678_NDUFA2
P25705_ATP5F1A
P16389_KCNA2
P22460_KCNA5
Q13303−3_KCNAB2
Z-score
1
0
−1
GOterm
Actin Cytoskeleton Signaling
Elastic fibre formation
Glutamate Receptor Signaling
Oxidative Phosphorylation
Potassium Channels

Fig. 2

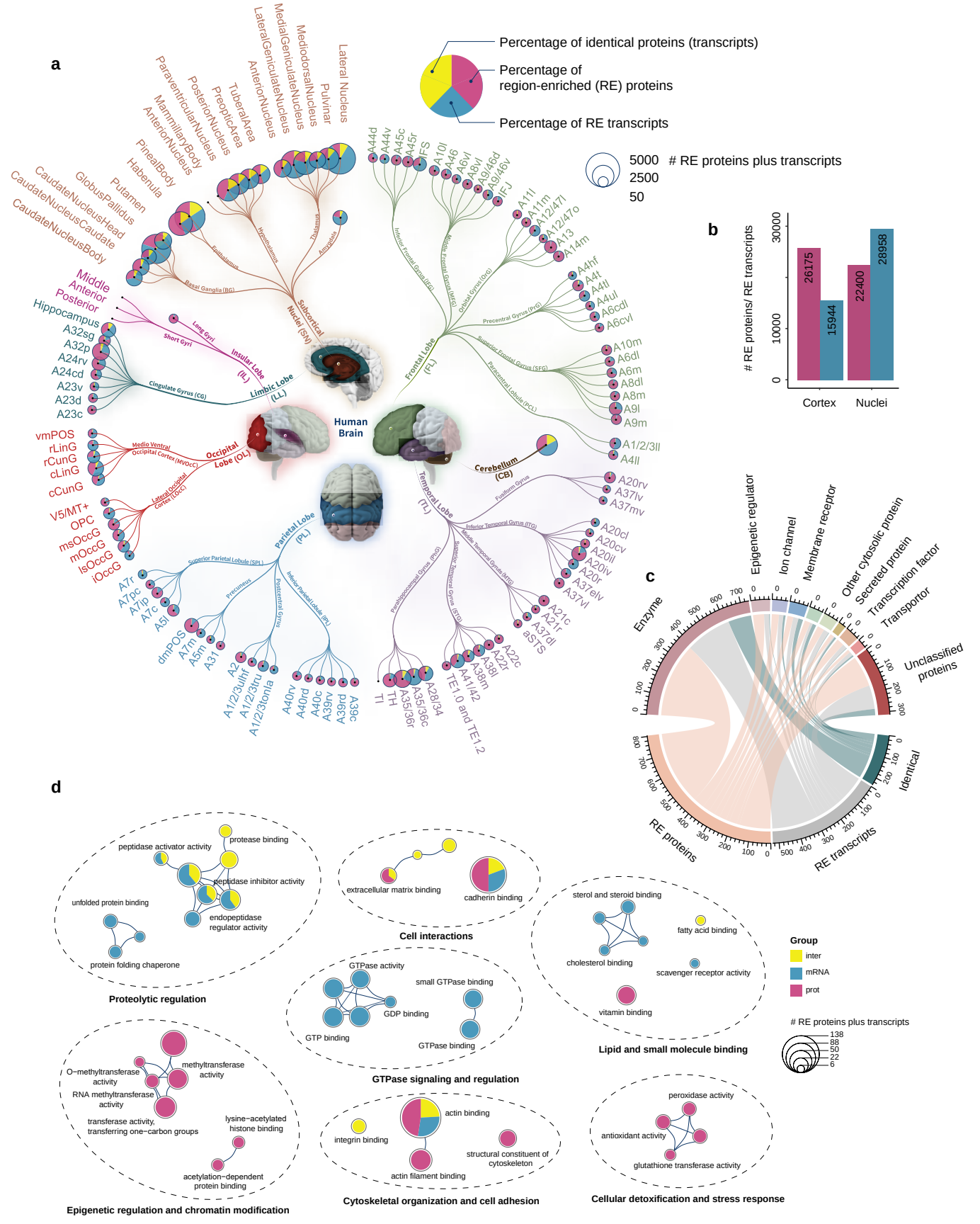
a
Percentage of identical proteins (transcripts)
Percentage of region-enriched (RE) proteins
Percentage of RE transcripts
5000
2500
50
RE proteins plus transcripts
Human Brain
Subcortical Nuclei (SN)
Frontal Lobe (FL)
Cerebellum (CB)
Temporal Lobe (TL)
Parietal Lobe (PL)
Occipital Lobe (OL)
Limbic Lobe (LL)
Insular Lobe (IL)
b
RE proteins/ RE transcripts
26175
15944
22400
28958
Cortex
Nuclei
c
Epigenetic regulator
Ion channel
Membrane receptor
Other cytosolic protein
Secreted protein
Transcription factor
Transportor
Enzyme
Unclassified proteins
Identical
RE proteins
RE transcripts
d
Proteolytic regulation
Cell interactions
Lipid and small molecule binding
GTPase signaling and regulation
Epigenetic regulation and chromatin modification
Cytoskeletal organization and cell adhesion
Cellular detoxification and stress response
Group
inter
mRNA
prot
RE proteins plus transcripts
138
88
50
22
6

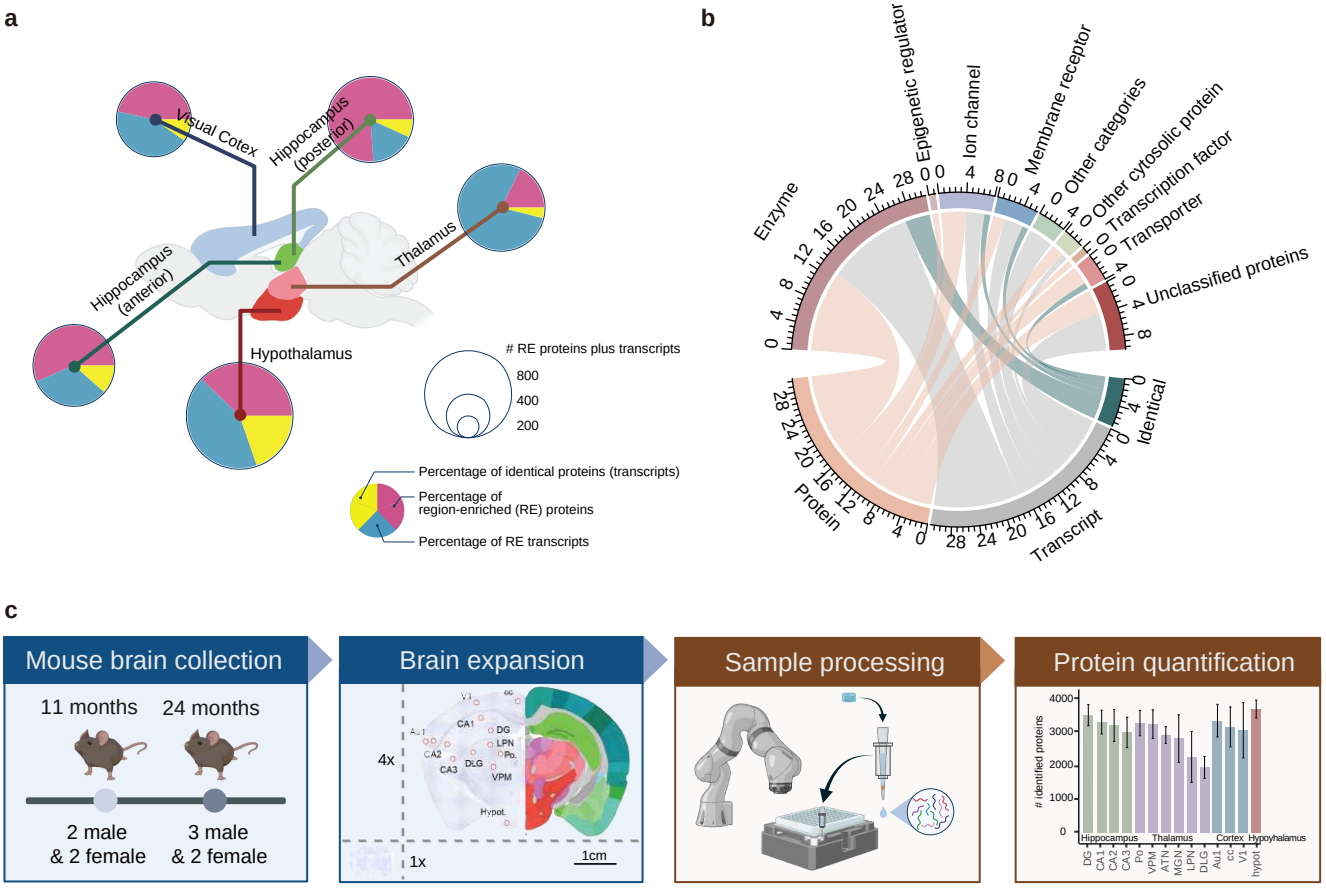
a
Visual Cotex
Hippocampus (posterior)
Thalamus
Hippocampus (anterior)
Hypothalamus
RE proteins plus transcripts
800
400
200
Percentage of identical proteins (transcripts)
Percentage of region-enriched (RE) proteins
Percentage of RE transcripts
b
Epigenetic regulator
Ion channel
Membrane receptor
Other categories
Other cytosolic protein
Transcription factor
Transporter
Unclassified proteins
Enzyme
Identical
Protein
Transcript
c
Mouse brain collection
11 months
24 months
2 male & 2 female
3 male & 2 female
Brain expansion
4x
1x
1cm
CA1
DG
LPN
Po
CA2
CA3
DLG
VPM
Hypot
Sample processing
Protein quantification
identified proteins
4000
3000
2000
1000
0
Hippocampus
Thalamus
Cortex
Hypothalamus
DG
CA1
CA2
CA3
Po
VPM
ATN
MGN
LPN
DLG
Au1
cc
V1
hypot

Fig. 4

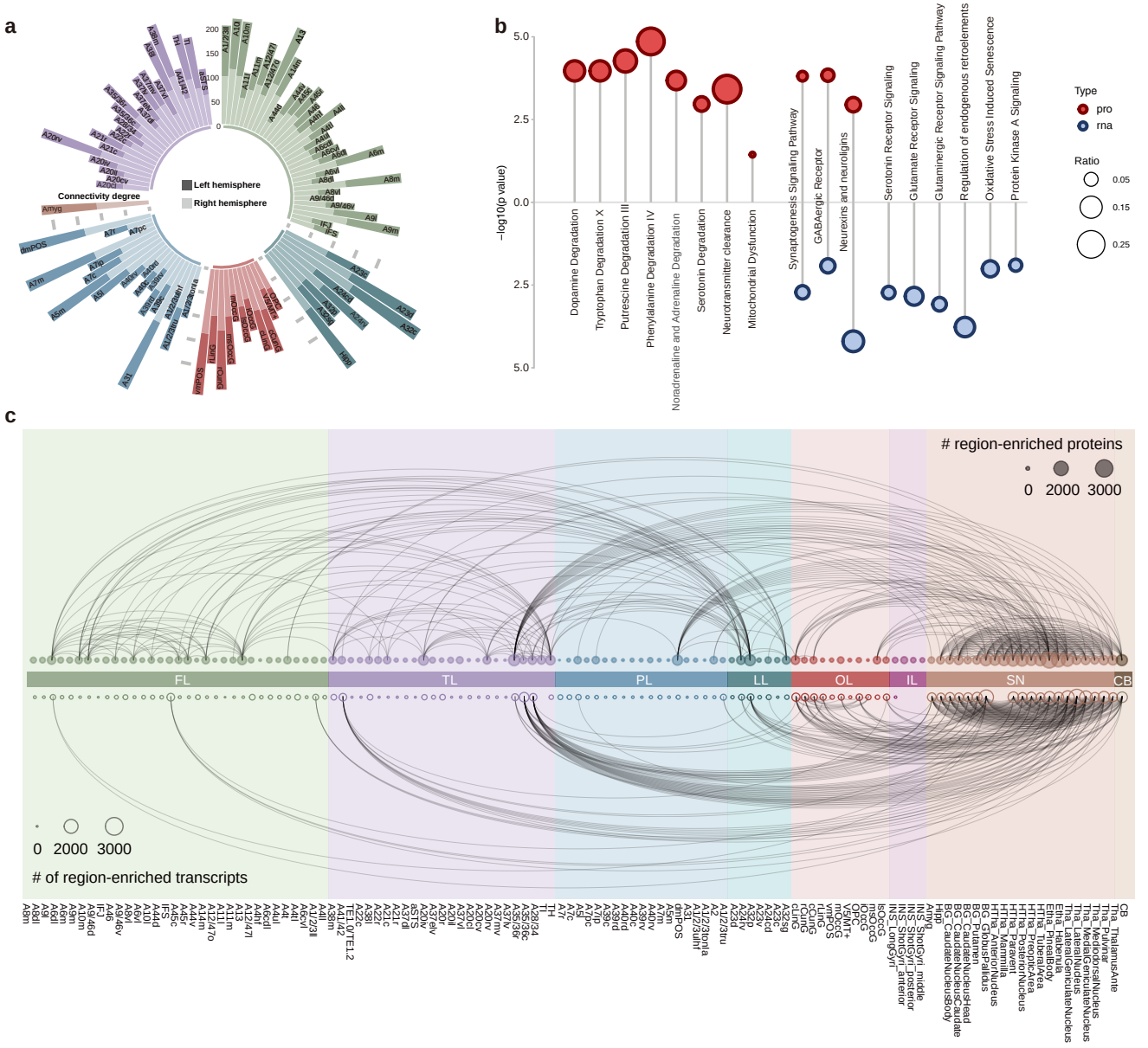
a
Left hemisphere
Right hemisphere
Connectivity degree
b
−log10(p value)
Dopamine Degradation
Tryptophan Degradation X
Putrescine Degradation III
Phenylalanine Degradation IV
Noradrenaline and Adrenaline Degradation
Serotonin Degradation
Neurotransmitter clearance
Mitochondrial Dysfunction
Synaptogenesis Signaling Pathway
GABAergic Receptor
Neurexins and neuroligins
Serotonin Receptor Signaling
Glutamate Receptor Signaling
Glutaminergic Receptor Signaling Pathway
Regulation of endogenous retroelements
Oxidative Stress Induced Senescence
Protein Kinase A Signaling
Type
pro
rna
Ratio
0.05
0.15
0.25
c
region-enriched proteins
0 2000 3000
FL
TL
PL
LL
OL
IL
SN
CB
0 2000 3000
# of region-enriched transcripts

Fig. 5

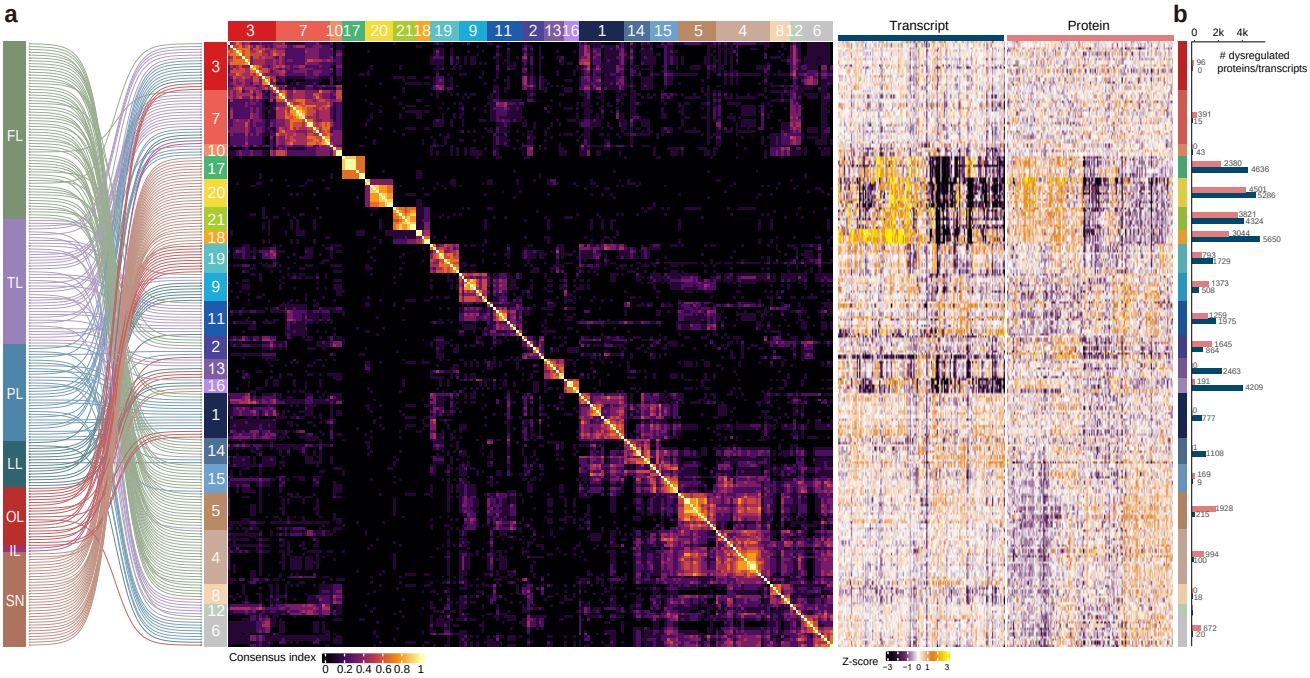
a
FL
TL
PL
LL
OL
IL
SN
Consensus index
0 0.2 0.4 0.6 0.8 1
Transcript
Protein
Z-score
−3 −1 0 1 3
b
dysregulated proteins/transcripts
0 2k 4k

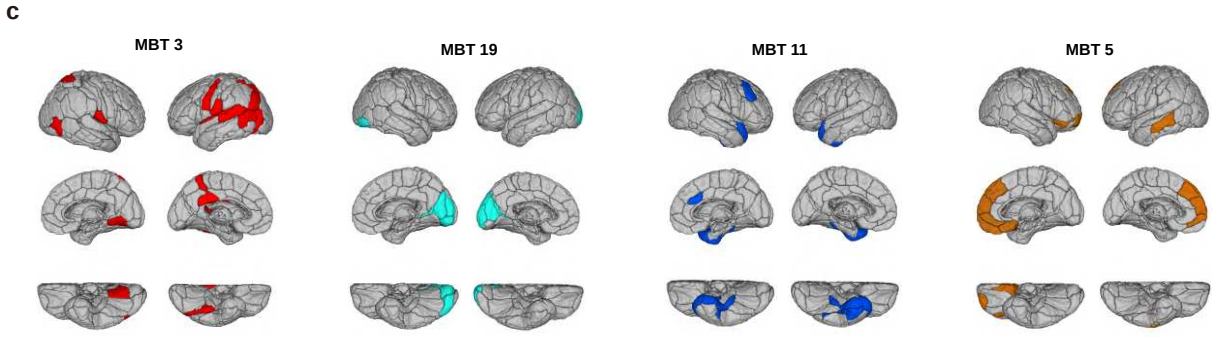
c
MBT 3
MBT 19
MBT 11
MBT 5

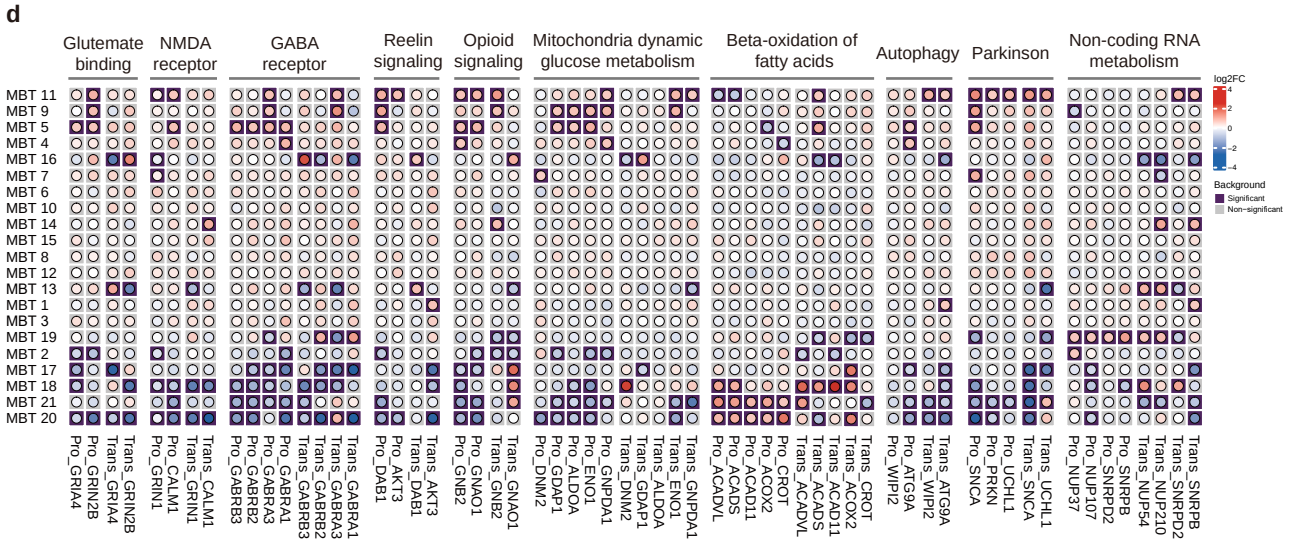
d
Glutemate binding
NMDA receptor
GABA receptor
Reelin signaling
Opioid signaling
Mitochondria dynamic glucose metabolism
Beta-oxidation of fatty acids
Autophagy
Parkinson
Non-coding RNA metabolism
log2FC
Background
Significant
Non−significant

Fig. 6

a

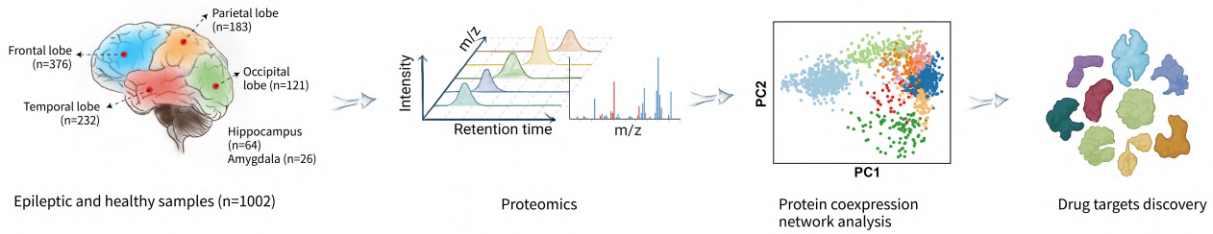
Parietal lobe (n=183)
Frontal lobe (n=376)
Occipital lobe (n=121)
Temporal lobe (n=232)
Hippocampus (n=64)
Amygdala (n=26)
Epileptic and healthy samples (n=1002)
Intensity
m/z
Retention time
m/z
Proteomics
PC2
PC1
Protein coexpression network analysis
Drug targets discovery

b

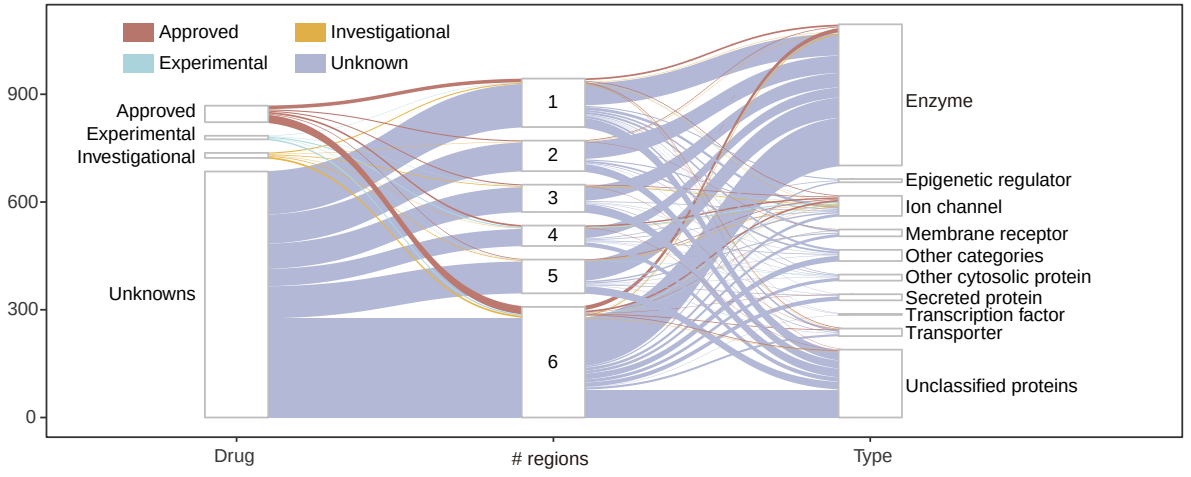
Approved
Investigational
Experimental
Unknown
900
600
300
0
Approved
Experimental
Investigational
Unknowns
1
2
3
4
5
6
Enzyme
Epigenetic regulator
Ion channel
Membrane receptor
Other categories
Other cytosolic protein
Secreted protein
Transcription factor
Transporter
Unclassified proteins
Drug
regions
Type

Supplementary Fig. 1

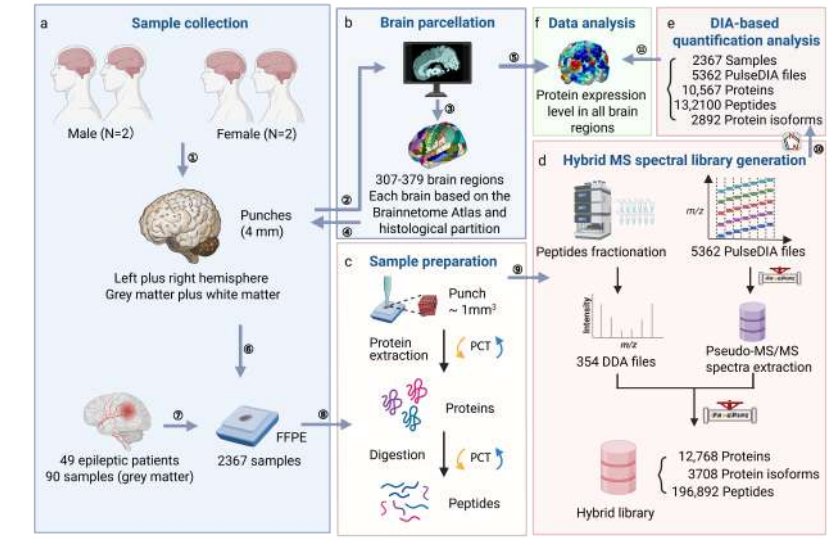

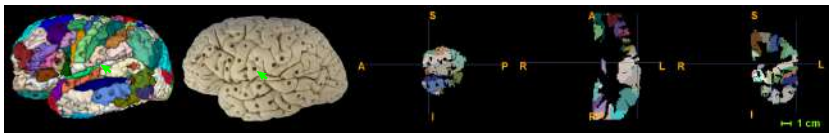

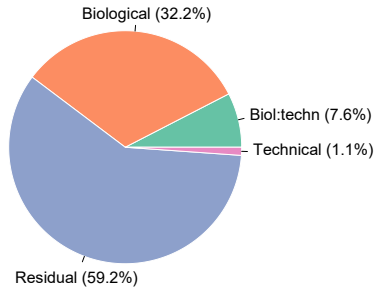

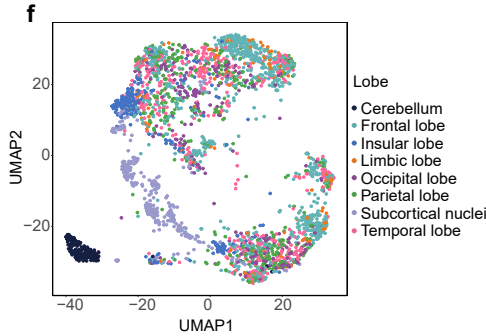

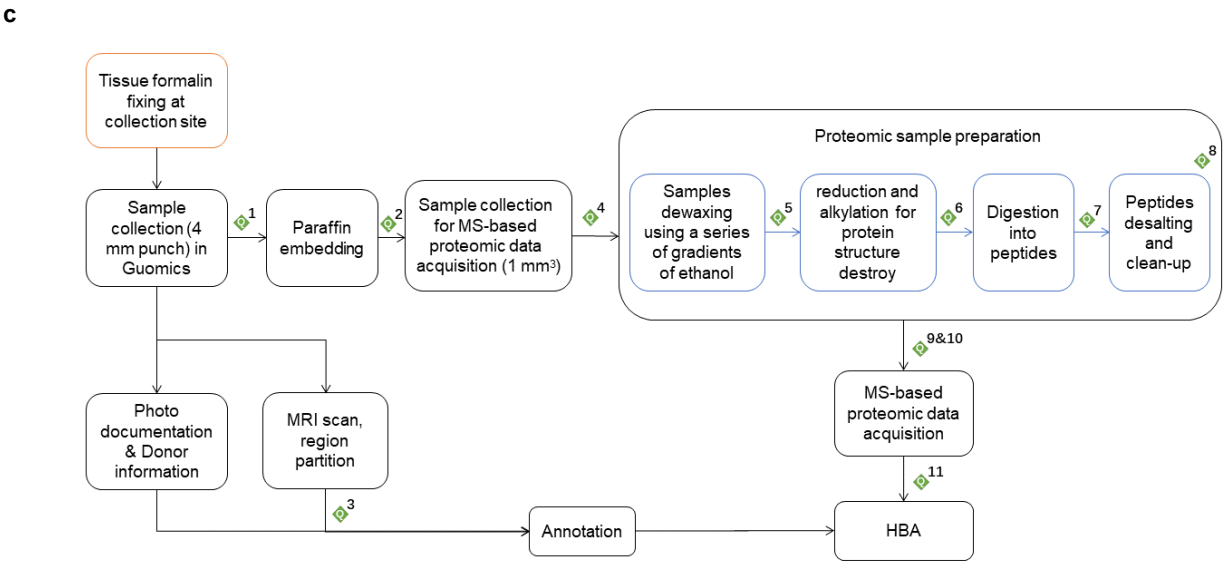

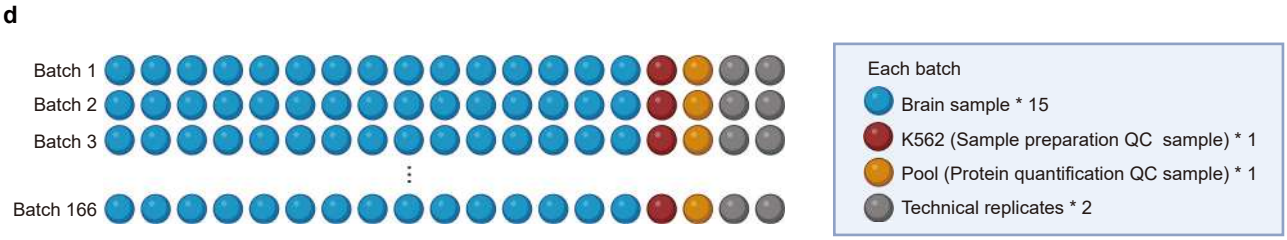

Supplementary Fig. 2

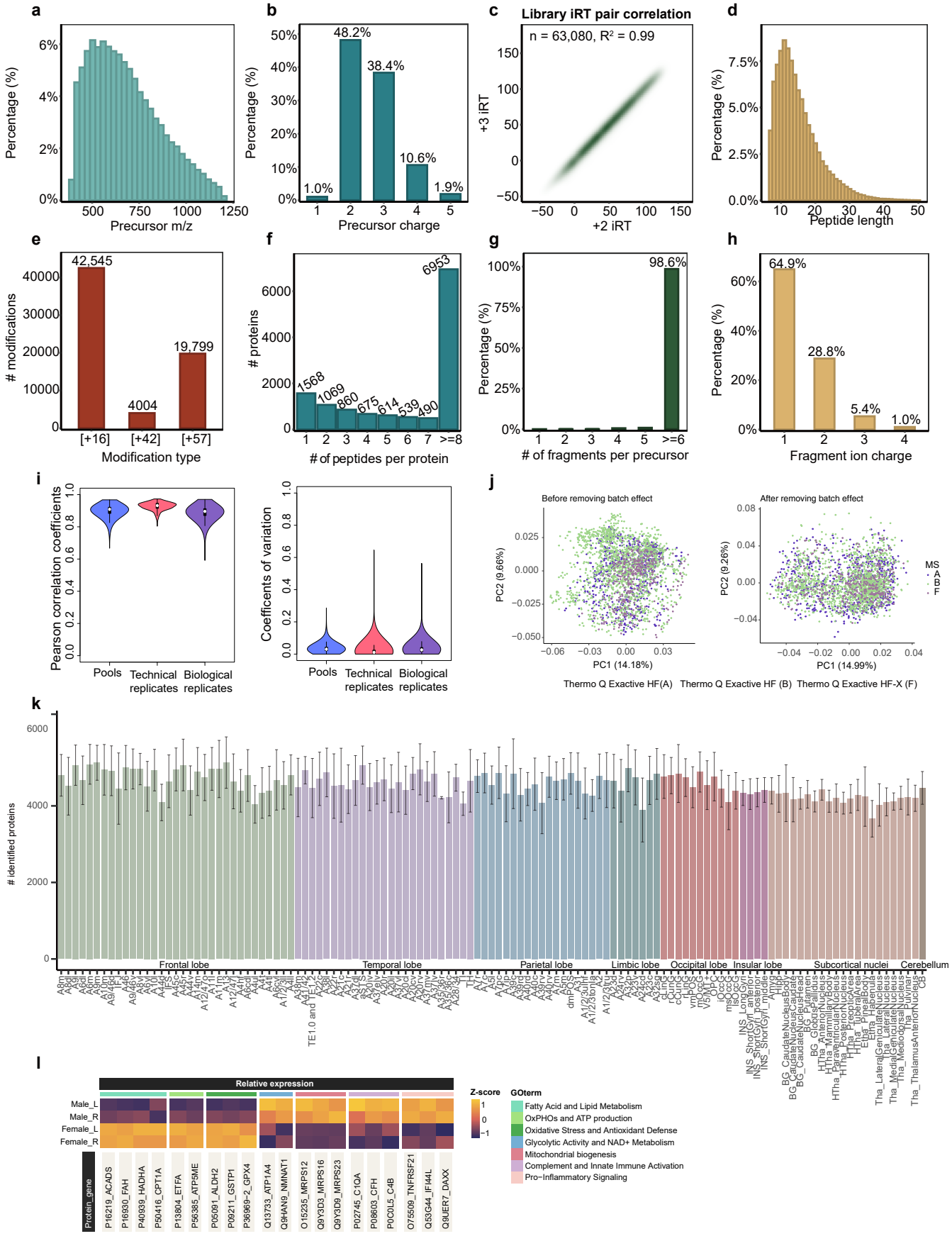

Supplementary Fig. 3

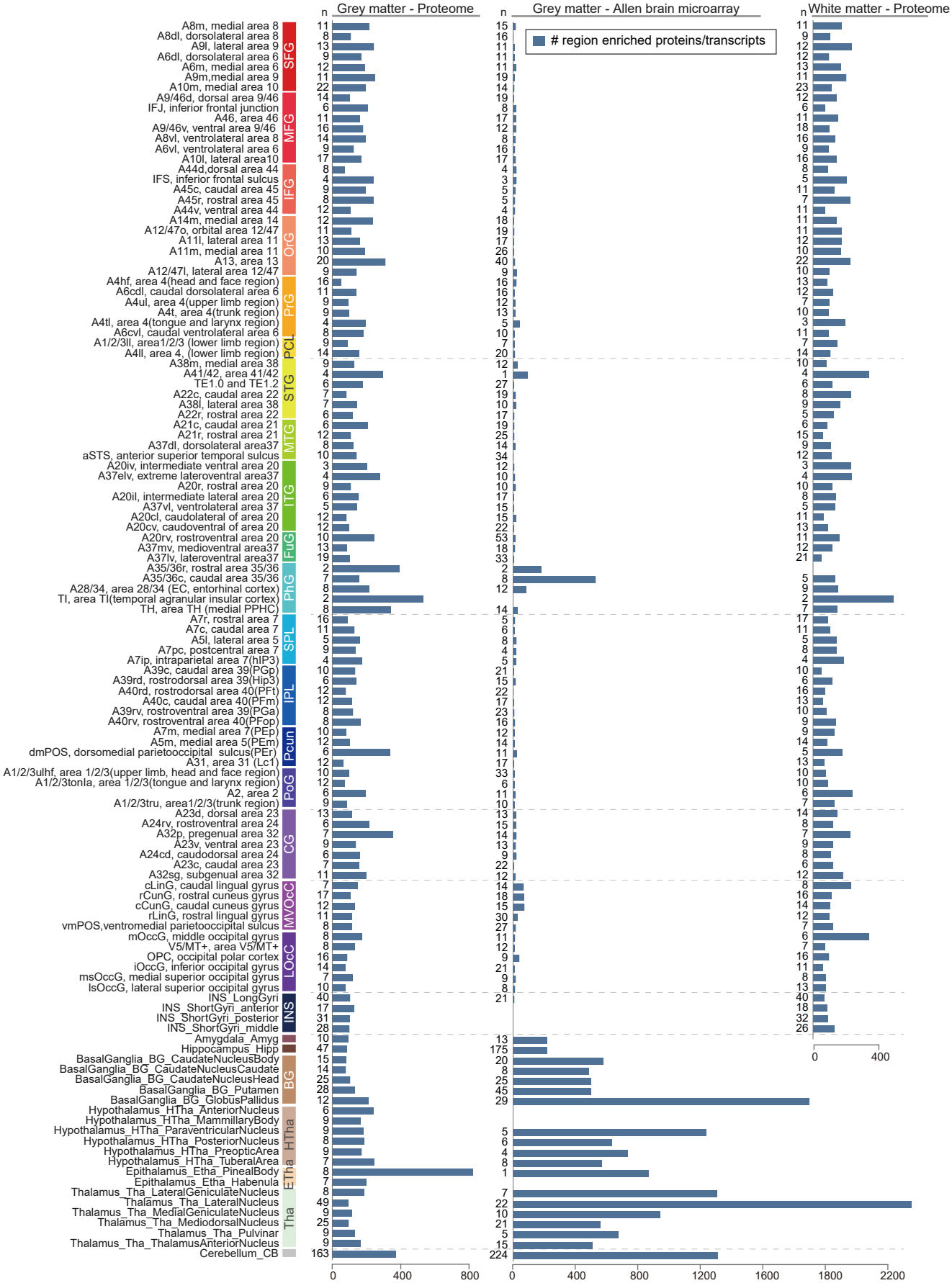

Supplementary Fig. 4

a

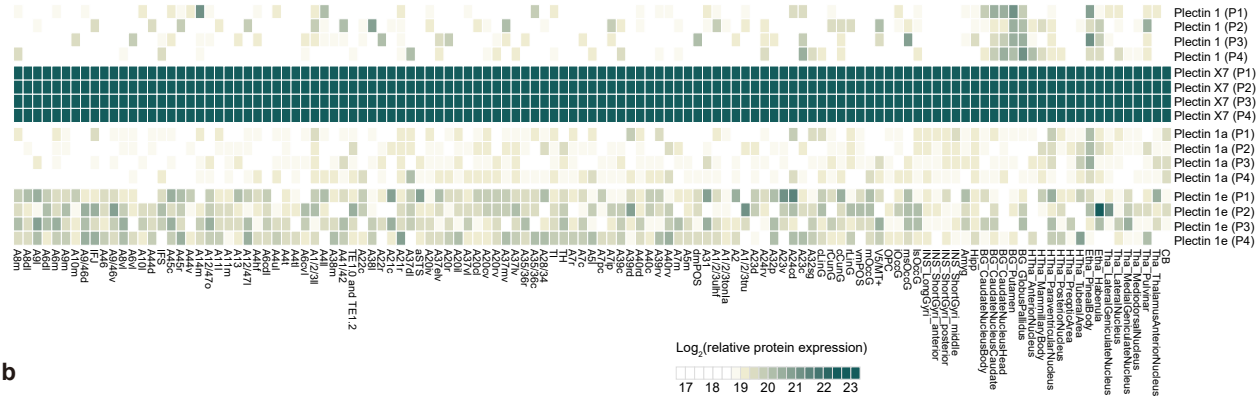

b

Supplementary Fig. 5

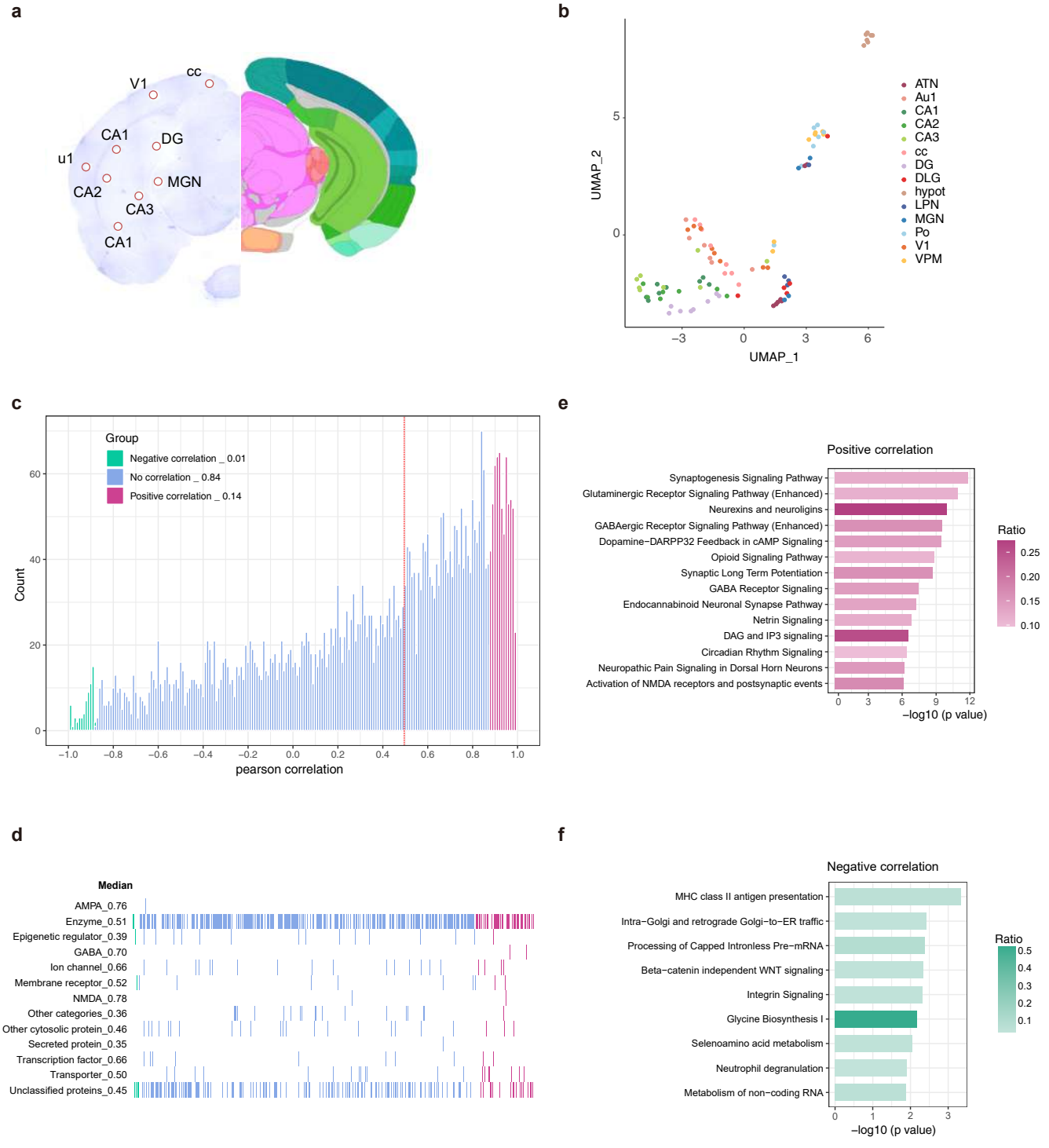

Supplementary Fig. 6

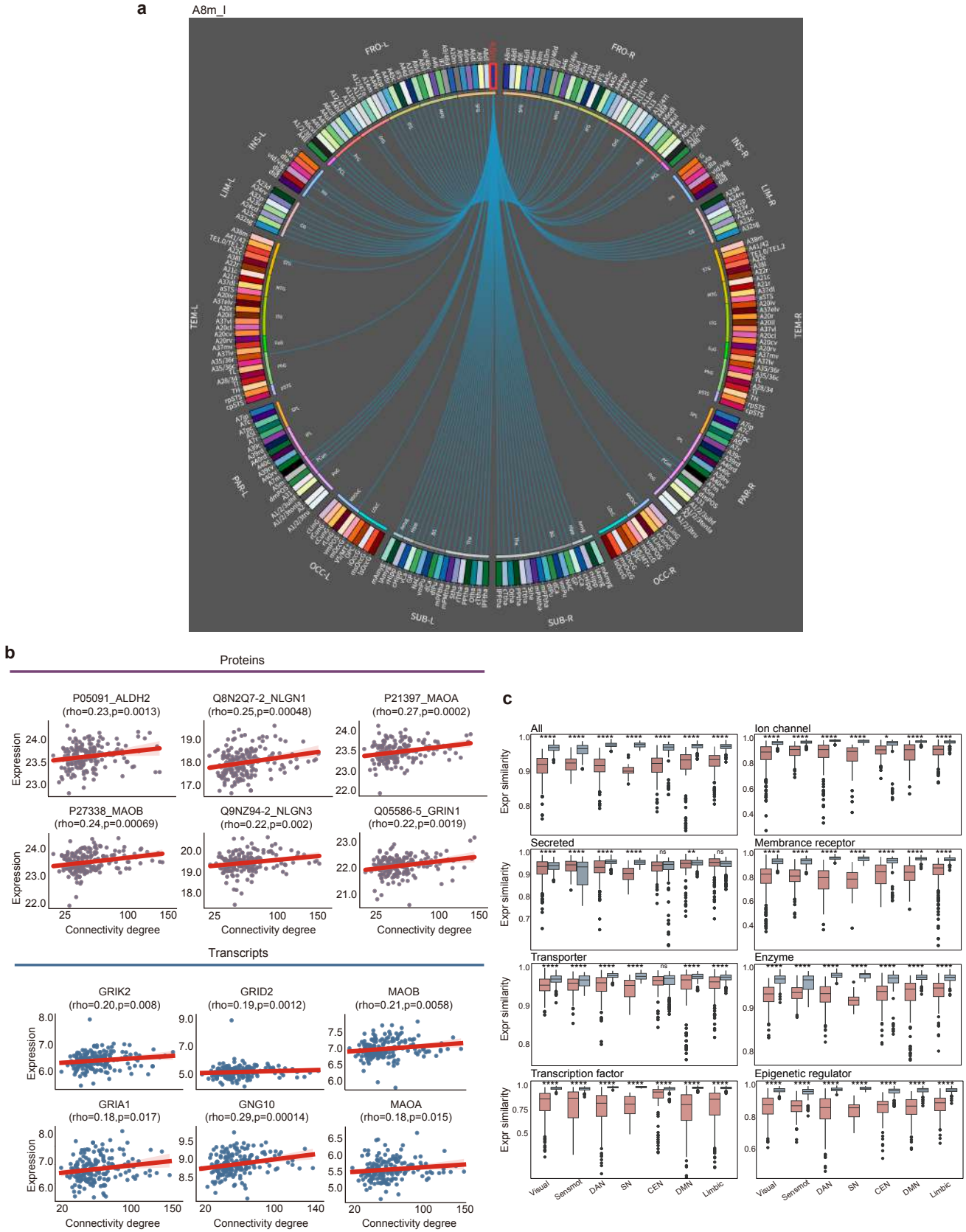

Supplementary Fig. 7

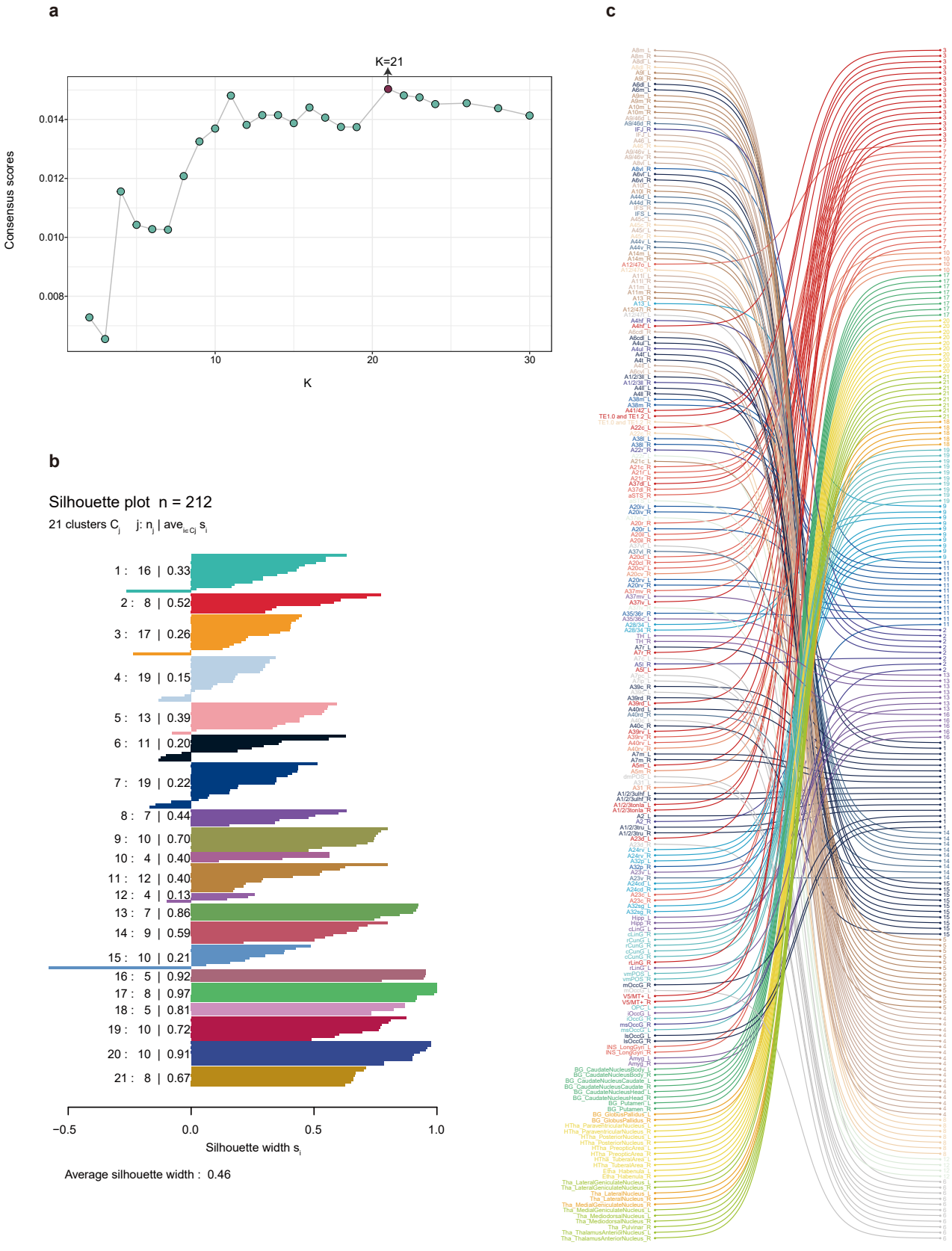

Supplementary Fig. 8

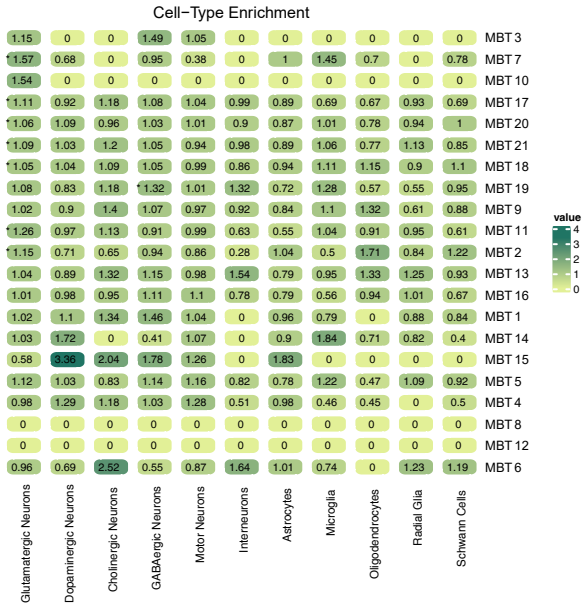

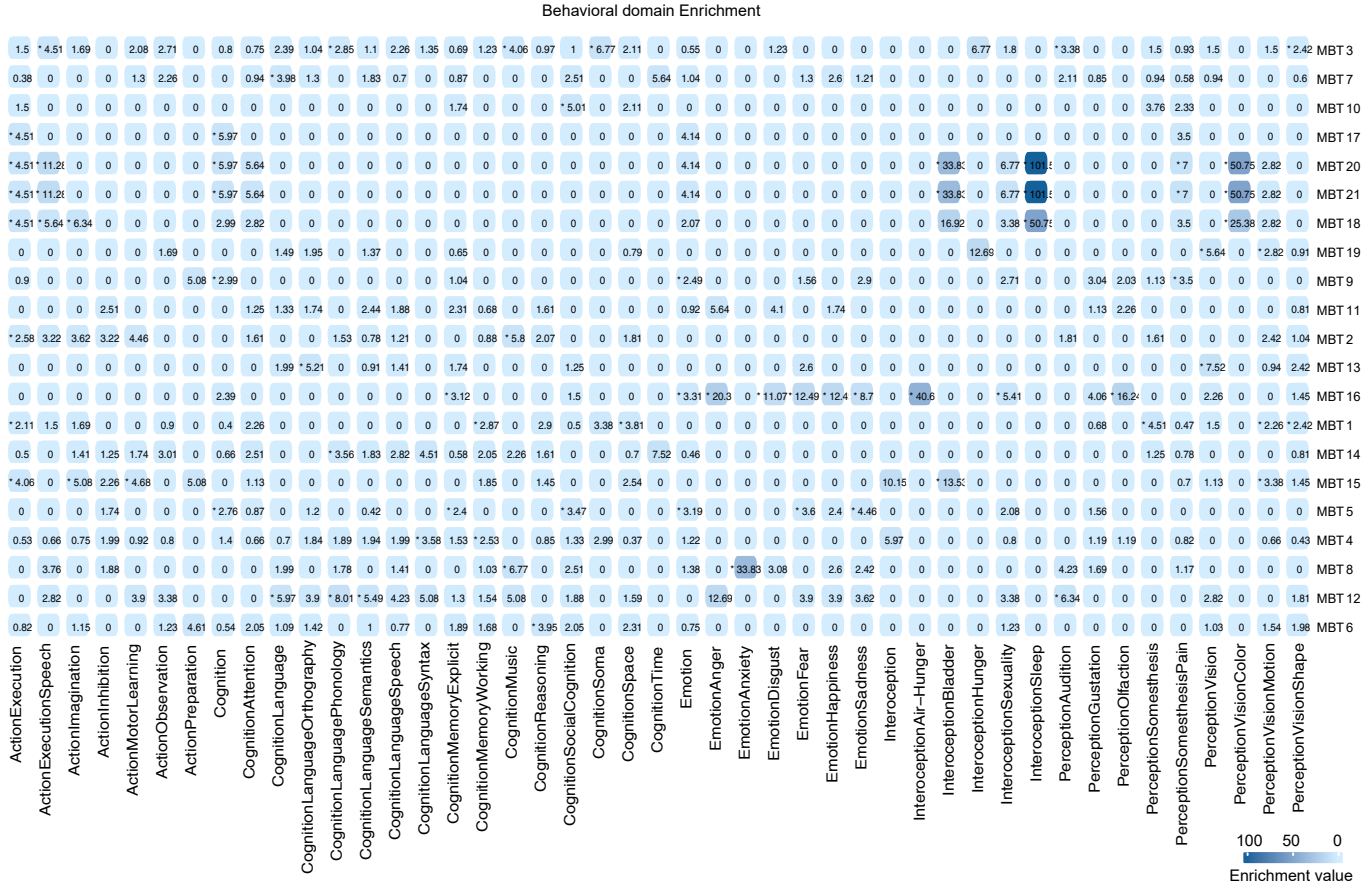

Supplementary Fig. 9

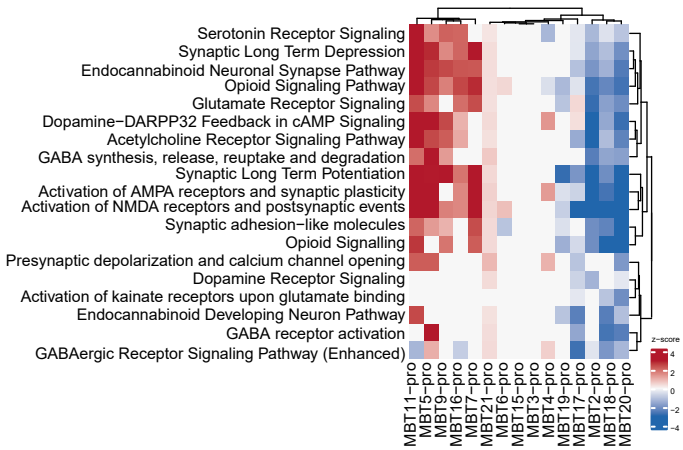

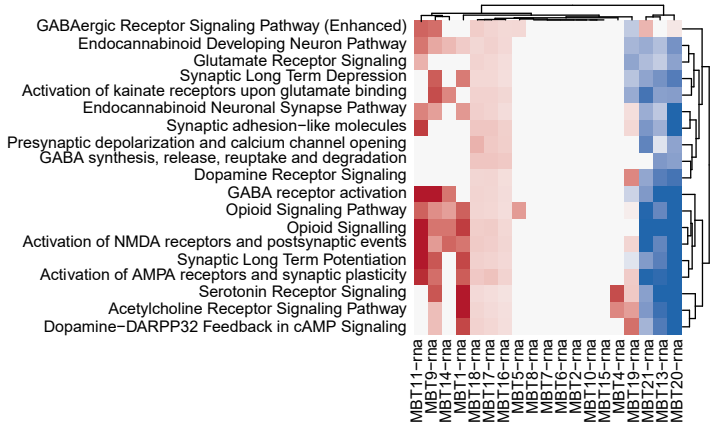

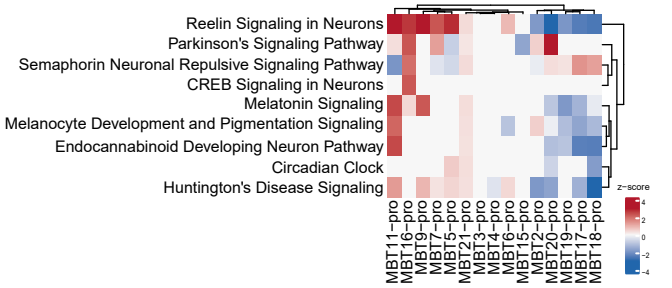

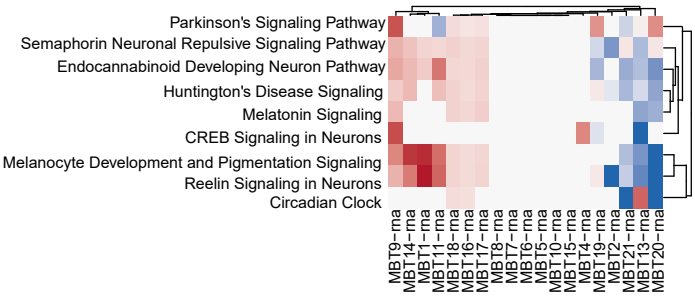

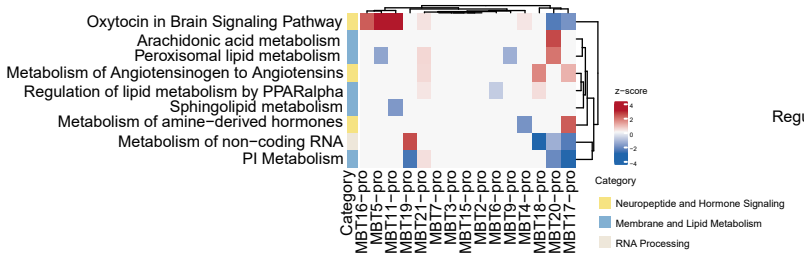

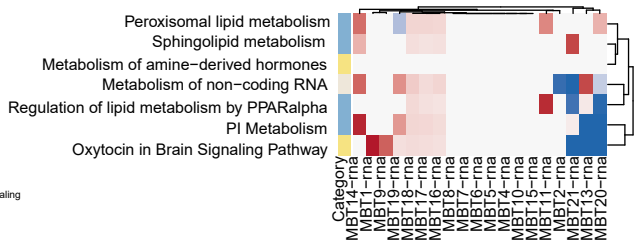

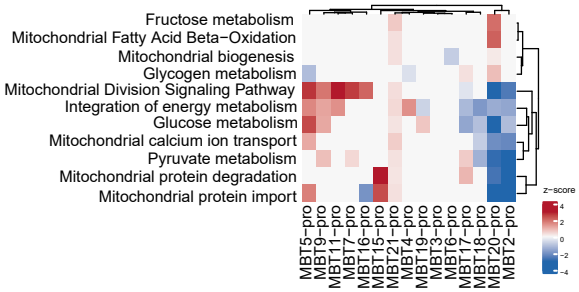

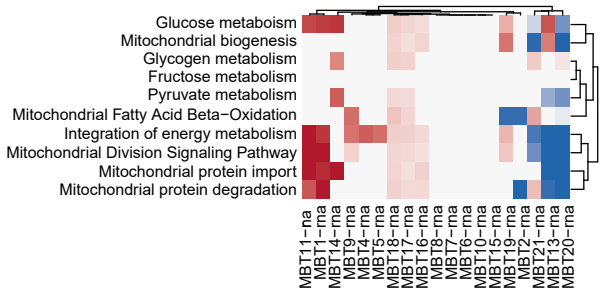

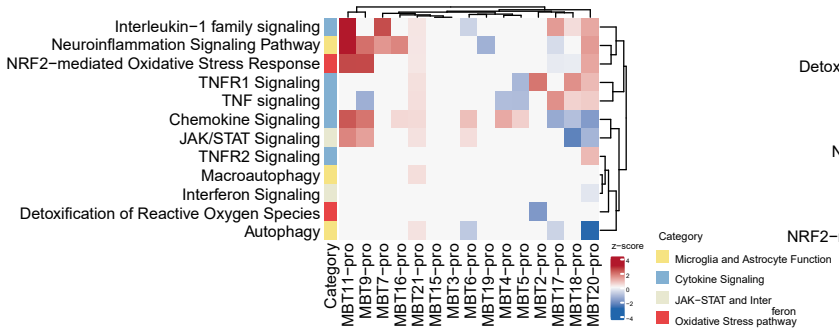

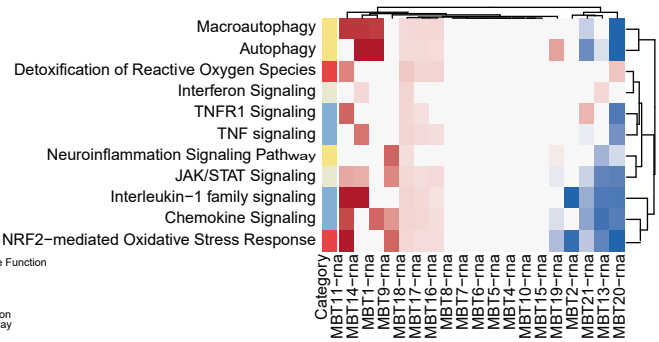

Supplementary Fig. 10

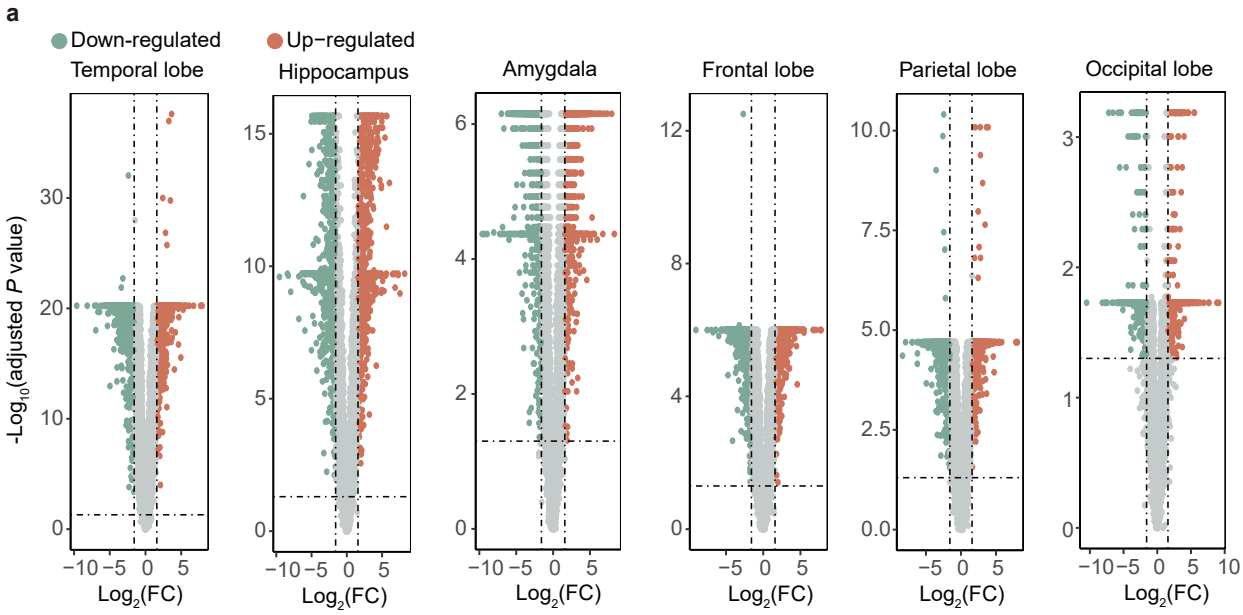

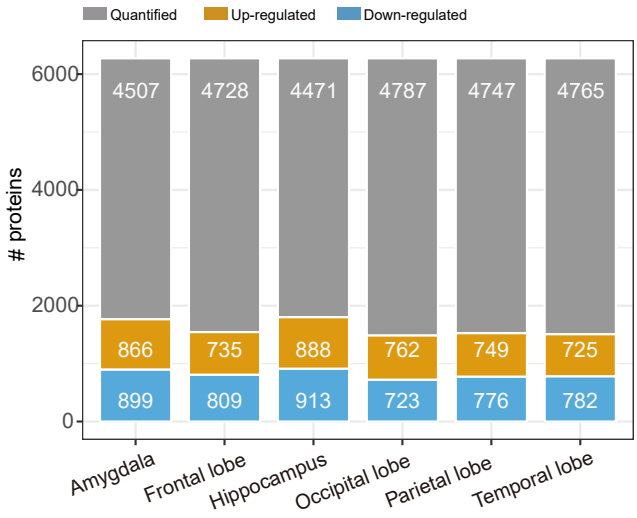

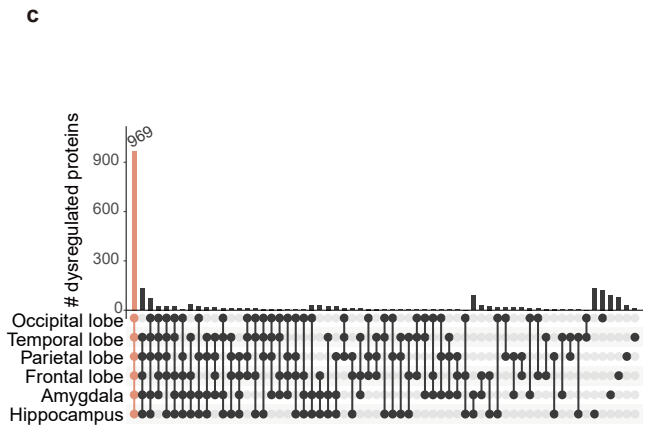

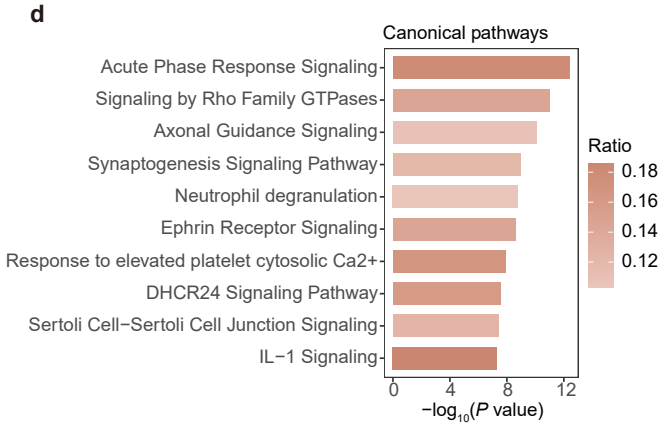

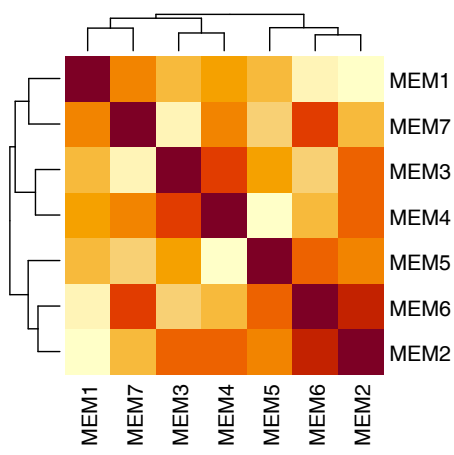

Supplementary Fig. 11

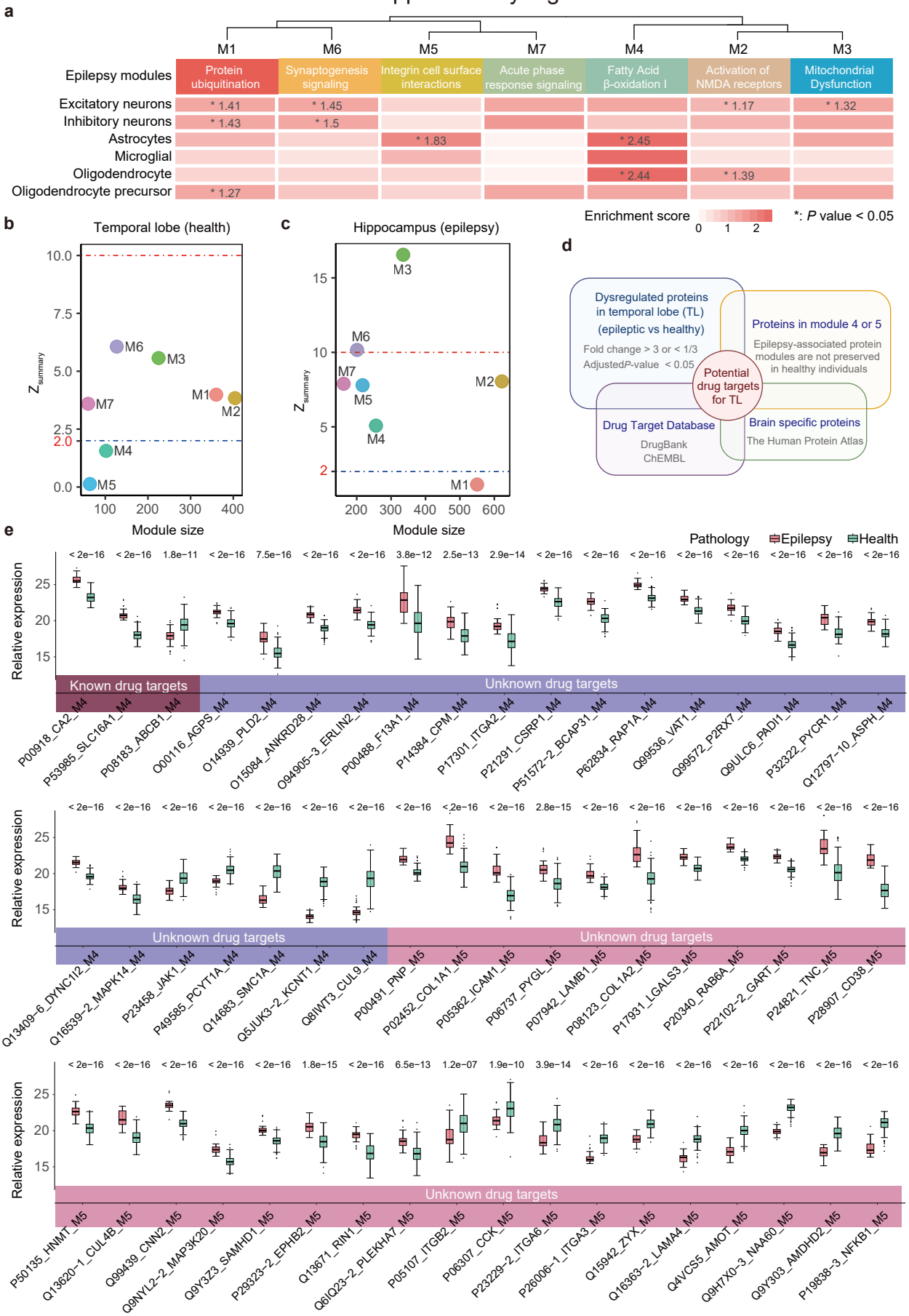
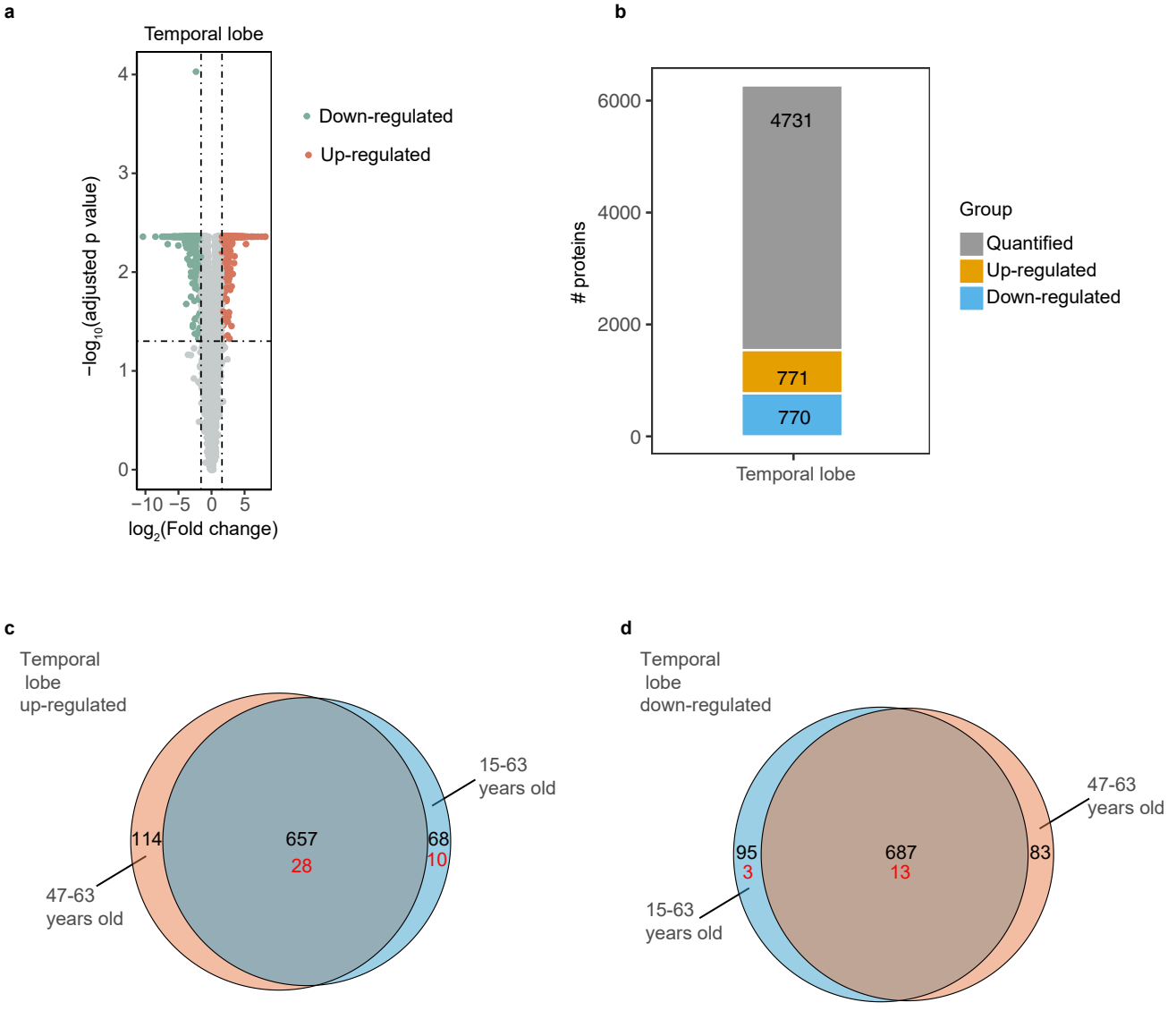
Supplementary Fig. 12